Chapter 3

Coal Characterisation and Oxidation Rate Measurements

3.1 Chemical and Physical Properties

3.1.1 Chemical Composition

Six of the sized coal fractions were analysed to determine if the chemical composition of the sample varied as a function of particle size. The results of these analyses are shown in Table 3.1 along with the bulk sample analysis for comparison.

Table 3.1. Ultimate and proximate analyses of Puxtrees coal fractions.

	0.125 mm	*0.428 mm*	*1.015 mm*	*2.25 mm*	*7.35 mm*	*9.0 mm*	*Bulk*
Moisture (%, adb)	2.9	2.9	2.9	2.9	2.6	2.7	2.5
Ash (%, adb)	5.0	3.6	4.0	3.6	4.0	3.3	3.5
Volatile Matter (%, adb)	36.3	37.8	37.5	37.9	38.9	38.6	36.5
Fixed Carbon (%, adb)	55.8	55.7	55.6	55.6	54.5	55.4	57.3
C (%, daf)	83.3	83.4	83.5	83.2	82.9	82.6	83.1
H (%, daf)	5.4	5.5	5.6	5.5	5.6	5.6	5.4
N (%, daf)	1.9	2.0	1.9	1.9	1.9	1.9	1.9
S (%, daf)	0.9	0.8	0.8	0.7	0.7	0.8	0.8
O (%, by diff, daf)	8.5	8.3	8.2	8.6	8.8	9.2	8.9
Calorific Value (MJ/kg, daf)	34.9	34.8	34.9	34.9	35.0	34.9	34.4

In general, the chemical composition of the sample was largely unaffected by the particle size of the material. The sulphur and nitrogen contents and H/C ratio were virtually constant over the full particle size range (Table 3.1 and Figure 3.1). In fact, the variation between samples shown in Table 3.1 was within or close to the limits of reproducibility quoted in the Australian Standard test methods (AS 1038 Part 2 – 1973; AS 1038.3 – 2000; AS 1038.6.1 – 1997; AS 1038.6.2 – 1997). The ash content of the 0.125 mm fraction was, however, slightly higher than the other fractions (Figure 3.1).

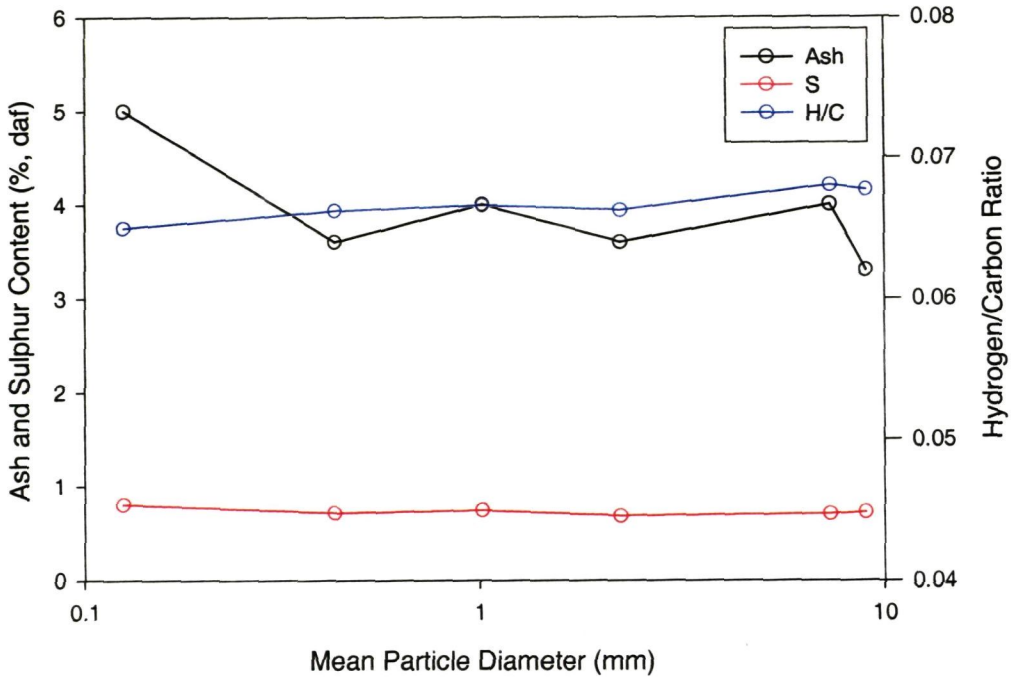

Figure 3.1. The dependence of chemical composition on particle size

These results compare well with those obtained by Palmer *et al.*, 1990, who also found that the chemical composition of low sulphur coals (i.e. about 0.3 to 0.4 percent total sulphur) was independent of particle size. Palmer *et al.* also found that the ash content of the coals examined increased with decreasing particle size, although in their study, the ash content varied over the entire size range examined. The coals in their study, however, were somewhat higher in ash than in this work (about eight percent compared to four percent in the Puxtrees coal) and covered a range of smaller particle sizes (2 mm down to -38 μm).

The concentration of ash in the finer particles is due to differences in the densities of the mineral and organic matter in the coal. The density of the coal is about 1.3 g/mL whereas the density of most minerals is around twice this value. As mineral matter is released from the organic matrix during crushing and sieving, it tends to separate and concentrate in the finer material. In this particular coal, the effects of the relatively large particle sizes (compared to the Palmer *et al.* study) and low ash content combined to largely avoid the effects of mineral separation.

The fact that the coal chemical composition can be considered constant over the entire particle size range is important for it means that differences in oxidation rates between different particle sizes are due to physical effects rather than differences in chemistry.

3.1.2 Petrology

The same six particle size fractions examined for chemical composition were also subjected to petrographic examination. The results of these analyses are summarised in Table 3.2.

Table 3.2. Results of the petrographic analyses of Puxtrees coal

Group	*Maceral*	*Volume (%)*					
		0.125 mm	*0.4025 mm*	*1.015 mm*	*2.25 mm*	*7.35 mm*	*9.0 mm*
Vitrinite	Telovitrinite	30.0	24.8	34.5	21.7	30.1	7.7
	Detrovitrinite	33.3	39.5	30.5	43.5	22.8	32.6
	Total	63.3	64.3	65.0	65.2	52.9	40.3
Liptinite	Sporinite	4.1	5.2	4.3	5.0	3.8	4.0
	Suberinite	Trace	trace	Trace	trace	trace	trace
	Resinite	0.3	1.0	0.6	0.3	0.1	0.5
	Cutinite	0.1	0.5	0.6	0.3	0.4	0.8
	Liptodetrinite	trace	trace	Trace	trace	trace	trace
	Total	4.5	6.7	5.5	5.6	4.3	5.3
Inertinite	Semifusinite	19.1	16.8	18.0	12.1	26.2	32.0
	Fusinite	3.4	2.0	2.0	2.6	3.3	2.0
	Macrinite	0.3	0.3	0.2	0.3	0.3	0.3
	Micrinite	trace	0.3	0.1	0.3	0.1	trace
	Inertodetrinite	7.8	6.7	7.6	10.3	10.2	16.5
	Total	30.6	26.1	27.9	25.6	40.0	50.8
Minerals		1.6	2.9	1.6	3.6	2.9	3.6

The petrographic composition of the coal was essentially the same for all fractions with particle diameters from 0.125 to 2.25 mm. Above 2.25 mm, however, the proportion of the vitrinite components decreased with a corresponding increase in the inertinite content of the fraction. There did not appear to be any significant change in the liptinite component across the range of particle sizes examined. The data are shown in graphical form in Figure 3.2.

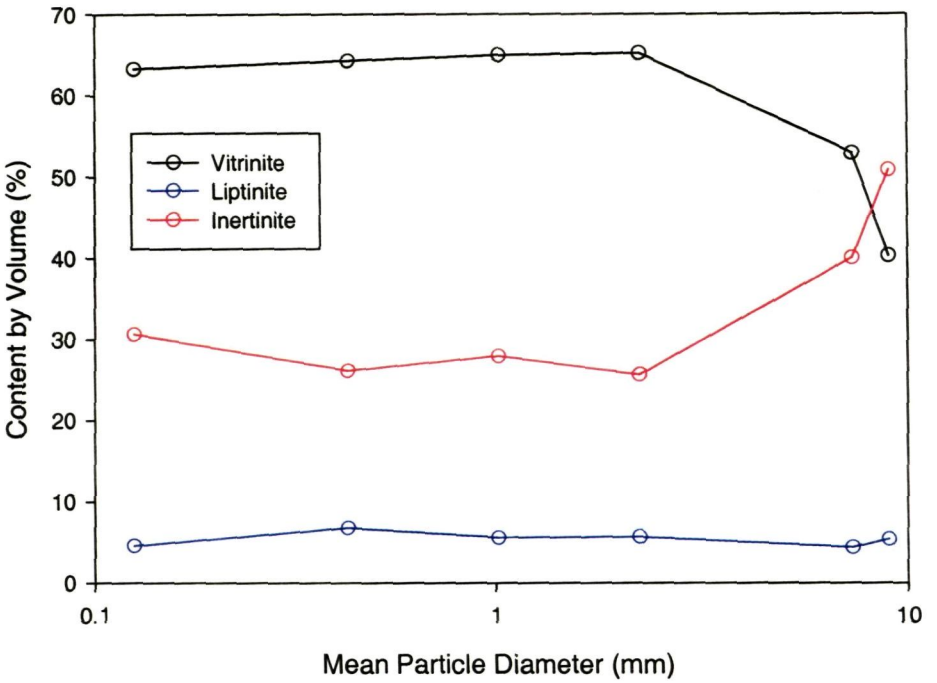

Figure 3.2. The dependence of petrographic composition of Puxtrees coal on particle size

The separation of macerals with particle size is a result of the crushing process. As discussed in Chapter 1, the physical and chemical properties of macerals in the same coal may be substantially different. Vitrinite is quite brittle and the layers of vitrain in which they occur are usually heavily fissured so that they are easily broken up during grinding (Teichmüller and Teichmüller in Stach *et al.*, 1982). Inertinite, on the other hand is usually much harder and more resistant to breakage. Since the vitrinite is easily broken down to smaller particle sizes it tends to concentrate in coal fines as the bulk coal is crushed.

3.1.3 Mercury Porosimetry

The volume of pores with radii greater than 3.75 nm was strongly dependent upon the mean particle diameter as shown in Figure 3.3. For 0.303 mm particles, the total intruded volume of 0.063 mL/g was more than 50 percent higher than the 7.3 mm particles with an intruded volume of 0.040 mL/g.

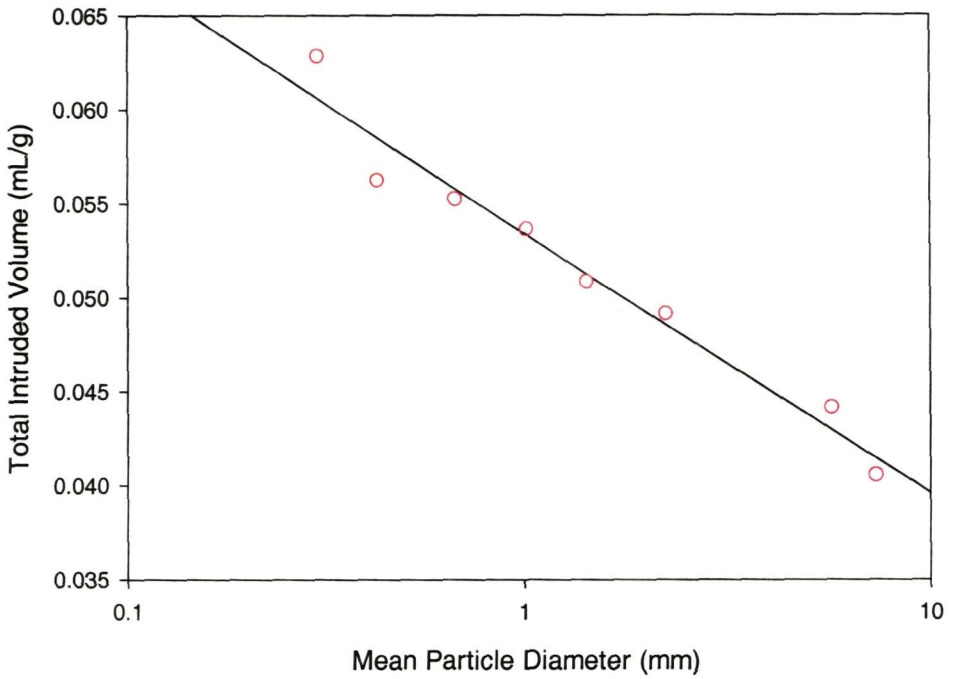

Figure 3.3. The dependence of total intruded volume on particle size

The reason for this is that most of the larger pores accessible to the mercury are on or near the surface of the particles. Towards the interior of the particles, these pores are not accessible because they are either not connected to the surface (i.e. blind pores) or the interconnecting pore network is too small for mercury to penetrate. For smaller particles, the external surface area per unit mass is much higher than for the larger ones so there is a proportionally higher number of relatively large accessible pores in small particles. In this particular coal, more than 35 percent of the accessible pores in the 0.303 mm particles were more than 100 nm in radius whereas for 5.73 mm material, only about nine percent were above 100 nm.

Compared to other coals, this material appears to be a medium to high porosity coal. Karsner and Perlmutter, 1981, measured the porosity of a number of American coals and found that the total intruded volume ranged from about 0.01 to 0.2 mL/g with most being below 0.1 mL/g. The particle size of their samples was between 2 and 3.5 mm. In more

recent work, Pànek and Taraba, 1996, examined a large number of Eastern European coals and found a similar range of porosities.

Although total intruded volume was a strong function of particle diameter, the surface area of the pores contacted by the mercury was about the same for all of the particle sizes, averaging at about 10.6 m^2/g. The reason for this apparent anomaly is that the large pores, which constitute a high proportion of the total pore volume in the smaller particle fractions, contribute little to the overall pore surface area. This effect is best illustrated by Figure 3.4 which shows the pressure-volume curves obtained for several particle size fractions.

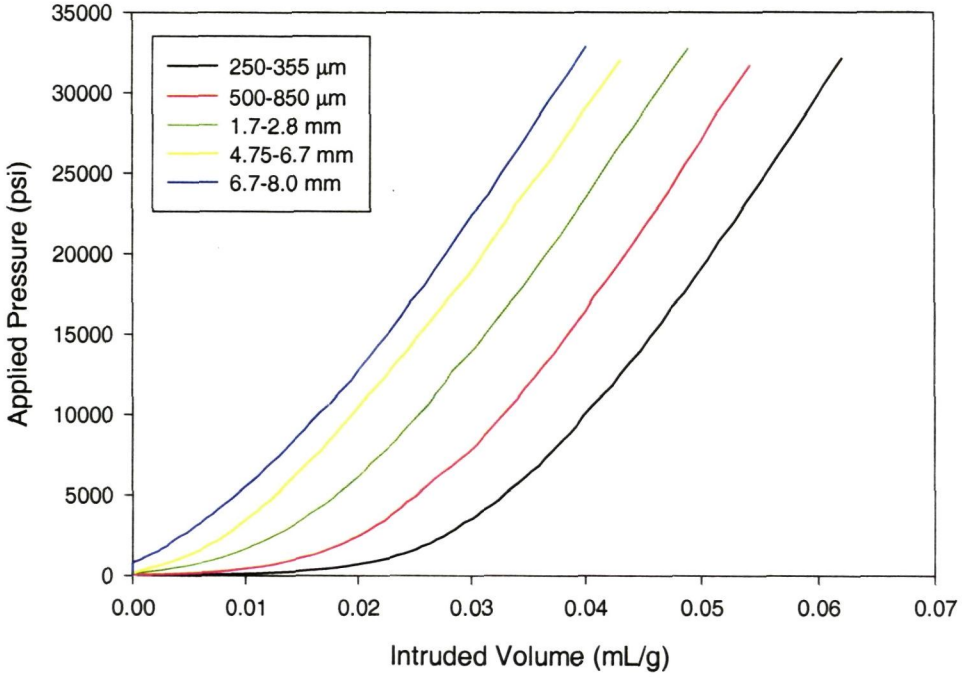

Figure 3.4. Mercury porosimetry pressure - intruded volume curves for various particles size fractions

At pressures below about 5000 psi, the contribution to the total intruded volume of the largest particles is quite small whereas for the finest material, more than half of the total intruded volume occurs in this region. Examination of Figure 3.4 shows that the area under the curves in this low-pressure region is contributing only a small proportion of the total area, although the total area bounded by each curve is similar for each size fraction. Since,

as explained in Chapter 2, the area under the pressure-volume curve is proportional to the pore surface area, it follows that the surface areas of each fraction must also be similar.

3.1.4 Helium Densities

The helium density of the coal appeared to decrease slightly with increasing particle size (Figure 3.5) varying from about 1.31 g/mL at 0.125 mm to 1.26 g/mL at 9.0 mm.

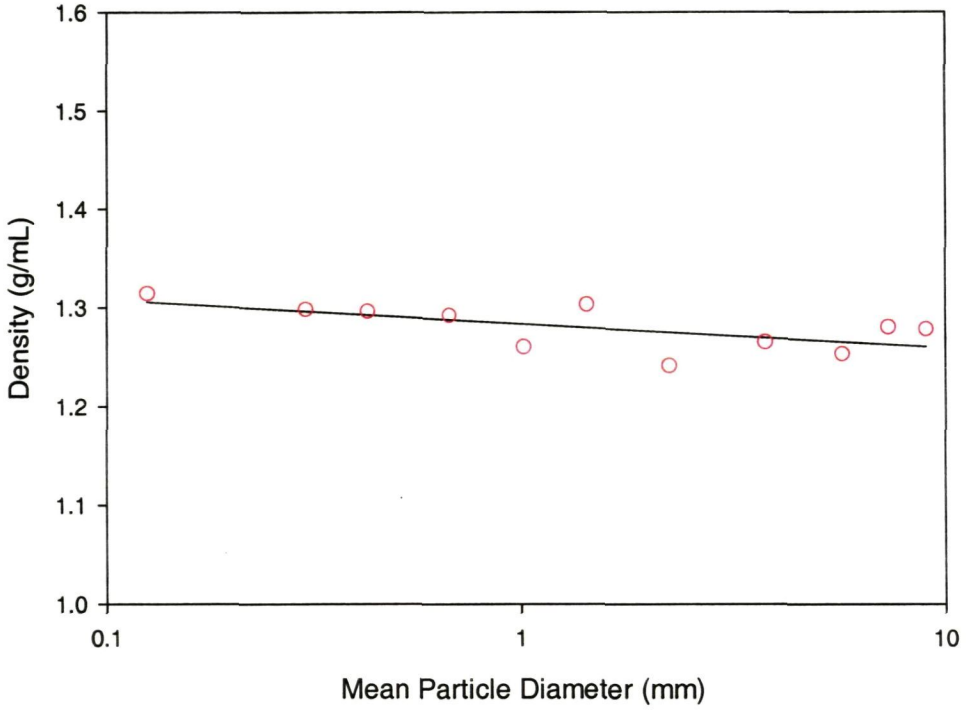

Figure 3.5. The dependence of helium density on particle size

This higher density of the finest material may be due in part to the slightly higher mineral content of these fractions. It is probably more likely, however, that the steady drop in density with particle size is due to helium being unable to access all of the internal void spaces in the larger particles. The effect of this is that these pores are not accounted for by the measurement technique so that the volume of the sample will be over estimated with the consequence that the measured density will be lower than the true density.

The mercury porosimetry results showed that the total intruded volume decreased from about 0.063 mL/g for the 0.125 mm particles to 0.040 mL/g for 7.3 mm particles. If it is

assumed that the volume of pores accessible to helium varies by a similar amount over this particle size range and that the true density of the coal is 1.3 g/mL, the measured density would vary from 1.3 to 1.26 g/mL. This agrees very well with the actual results and indicates that a significant proportion of the internal pore structure is inaccessible in the larger particles.

3.1.5 CO_2 Surface Areas

The CO_2 surface areas of six particle size fractions were determined using the Dubinin-Radushkevich model described in Chapter 2. The results of these measurements are shown in Figure 3.6.

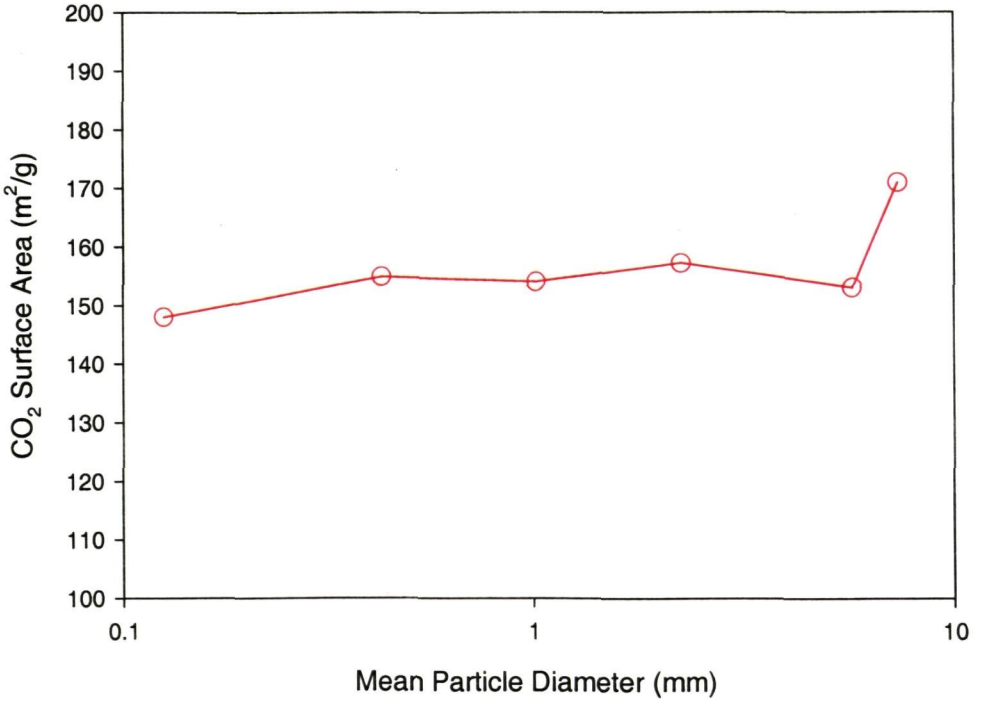

Figure 3.6. The dependence of CO_2 surface area on particle size

The internal surface area of this coal measured by this technique was not greatly affected by the particle size within the range of 0.125 mm to about 6 mm, averaging at about 150 m^2/g. This suggests that most of the internal porosity of the coal is accessed by the CO_2 molecules regardless of the particle diameter. This contrasts with the results of the mercury

porosimetry and helium pycnometry results which indicated that access to the internal pore structure was diminished in larger particles. Carbon dioxide is known to be soluble in coal and it has been suggested by Larsen *et al.*, 1995, that it is this solubility that gives rise to the much higher surface area normally reported for coals by CO_2 compared to other adsorbates. They contend that the pore structure is not necessarily interconnected but rather, CO_2 diffuses through the solid to reach the micropore surfaces which would otherwise be inaccessible to insoluble adsorbates. Their model appears to be consistent with the results of the current study.

Surprisingly, the surface area of the largest particles (7.35 mm) was nearly 15 percent higher than the other fractions. This fraction had a high inertinite content with a correspondingly lower vitrinite content compared to the finer material. Inertinites are derived from plant material which was been subjected to severe biochemical alteration before being buried (Smyth, 1990) and, as a result they are often more porous than vitrinites which were protected from alteration. Higher porosity may lead to higher internal surface areas (R. Sakurovs, personal communication).

The results of these measurements are rather different from those found by some other groups who have examined surface areas as a function of particle size. Itay *et al.*, 1989, found that the surface area of a South African coal decreased linearly from about 90 m^2/g for 45 μm particles to around 35 m^2/g for 500 μm particles. Palmer *et al.*, 1990, in a study of Canadian coals with particle diameters from 22 μm to 1.1 mm also found that the CO_2 surface area decreased with increasing particle diameter although they noted that there appeared to be a levelling off at 50 μm. In both cases, the apparent reduction in internal surface area was attributed to the adsorbate gas being unable to access the entire pore network. An alternative explanation, described below, may be that the particle size effects

observed by the Itay and Palmer groups may have been an artefact caused by the measurement technique they used.

Both of these groups used a common technique in which a mixture of the adsorbate, CO_2, and a helium carrier gas flows over a sample that is maintained at the adsorption temperature. The composition of the gas passing over the sample varies as CO_2 is adsorbed but eventually reaches an equilibrium once adsorption is complete. Equilibrium is judged to be reached when the rate of change of the gas composition is very low and typically, the time required to reach this point may be less than 45 minutes. The procedure is repeated at various partial pressures of CO_2 so than an isotherm can be constructed from which the surface area is calculated.

The measurement technique used in the current study relied on a different principle in which successive aliquots of CO_2 were injected into the sample cell and the pressure was monitored to determine the volume of CO_2 adsorbed (Chapter 2). In this case, however, the time taken to reach equilibrium was much higher than 45 minutes even though the mass of sample used was comparable to that used in the dynamic system. The time required to reach equilibrium was a strong function of particle size and varied from about 9 hours for the 0.125 mm sample to more than 44 hours for the 7.35 mm particles. The rate of adsorption (and probably dissolution) of CO_2 by the coal is therefore quite slow and the relatively short equilibration time used in the gas flow method appears to have been insufficient to allow complete coverage of the surface.

To test this, the surface areas of two fractions of coal were measured using a Quantasorb Surface Area analyser which works on the gas flow principle. The results are shown in

Table 3.3 together with the corresponding values obtained with Micromiretics the instrument (which uses the aliquot method).

Table 3.3. Comparison of surface ares determined by the two measurement techniques

Size Fraction (mm)	*Aliquot Method (m^2/g)*	*Flow Method (m^2/g)*
0.125	145	63.1
1.0	154	44.5

The surface areas obtained with the flow apparatus were much lower than those from the aliquot method. As well, the surface area of the 0.125 mm material is apparently about 50 percent higher than that of the 1 mm particles when measured on the flow instrument. This can be contrasted with the aliquot method where the surface area is slightly larger for the larger particles compared with the finer material.

These results tend to confirm the view that equilibration times of the order of hours are needed in any surface area measurement technique to enable the adsorbate to reach all of the internal pore structure. Shorter times may yield results which underestimate the true surface area, particularly for larger particles.

3.2 Oxidation Kinetics

Low temperature oxidation of coal is predominantly due to the reaction of the organic matrix of the coal with ambient oxygen, however, some minerals, and in particular pyrite, also react with oxygen. Ritchie, 1994, quoted a number of experimentally measured oxidation rates for pyrite which, within the level of uncertainty, were approximately the same as coal. Hence, if the mineral content of the coal is high, the measured oxidation rate for the sample may include a significant contribution from the oxidation of these minerals that may complicate interpretation of the oxidation measurements.

In this study, an attempt was made to estimate the extent to which pyrite could affect the results. The pyrite content of the sample was estimated from the total sulphur, which

includes pyritic sulphur, and the iron content of the ash (7.5 percent, from the 1999 Coal Report for coal from the same source as the Puxtrees sample). The ash content of the coal was less than four percent (Table 3.1), so the available iron limited the pyrite content to a maximum of about 0.4 percent. This accounts for about 25 percent of the total sulphur in the coal, the remainder presumably being present as sulphate minerals or in organic form.

Assuming that the oxidation rate of pyrite is the same as the organic material, a pyrite content of 0.4 percent would only account for less than 0.5 percent of the measured rate. For the purposes of this study, therefore, the oxidation reaction was considered to be due solely to the oxidation of the organic material.

Over 50 experiments were performed in which the rate of oxidation of the Puxtrees coal sample was measured over a range of particle size fractions, temperatures, oxygen partial pressures and moisture contents. The effects of the various parameters are discussed below.

3.2.1 Effect of Time

In all of these experiments the characteristic decrease in oxygen consumption with time (Figure 3.7) was observed. The rate of oxygen consumption tends to approach a limiting value but apparently does not actually stop altogether. In one experiment using the full range coal sample, the rate was measured at ambient temperature (22 °C) and even after 60 days oxygen was still being consumed.

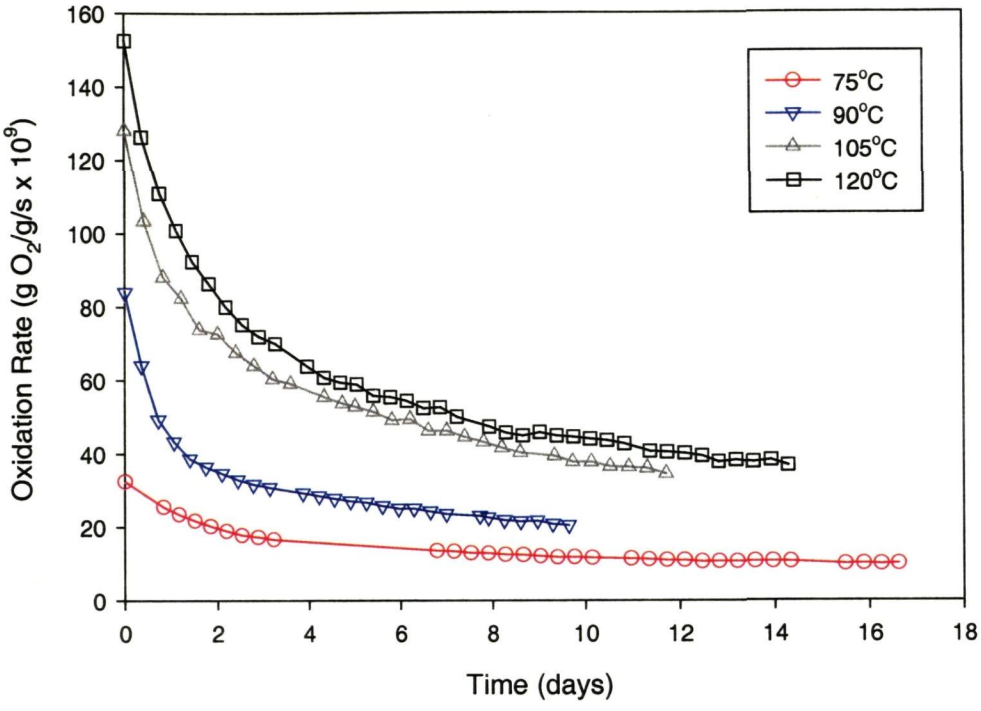

Figure 3.7. Oxidation rate as a function of time for 8-10 mm particles of Puxtrees coal

3.2.2 Effect of Temperature

Figure 3.8 compares the oxidation curves for the full range material (i.e. < 32 mm) measured at temperatures from 22 °C to 120 °C.

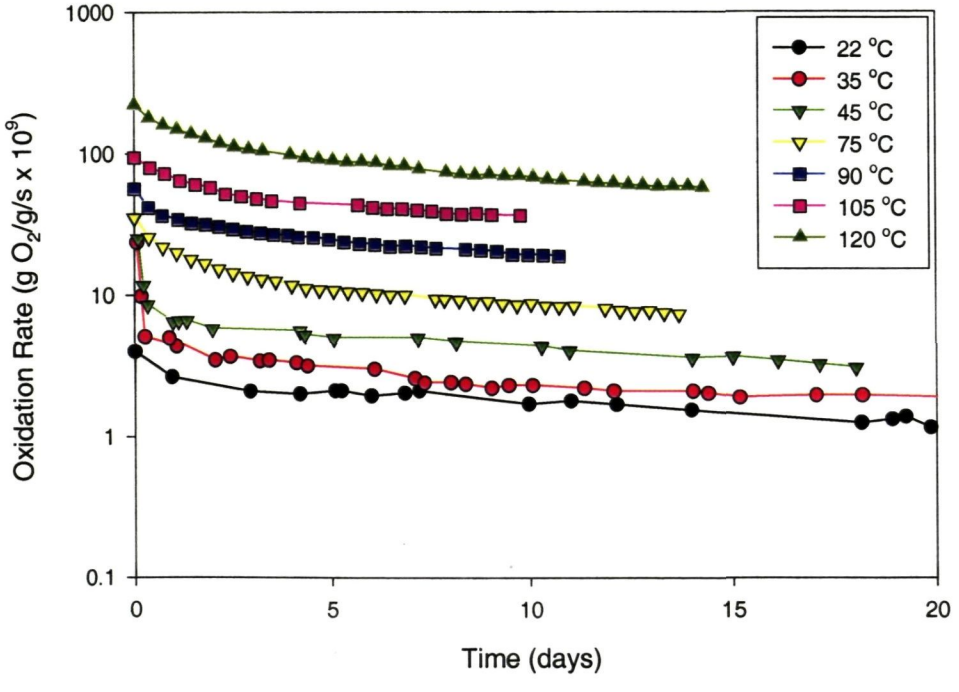

Figure 3.8. Oxidation rate as a function of time for the full range material at temperatures from 22 to 120 °C

In common with most other work, the temperature dependence was well described by the Arrhenius equation (Equation 1.5). Plots of $ln(R_O)$ versus $1/T$ were linear over the temperature range of 22 to 120 °C (Figure 3.9).

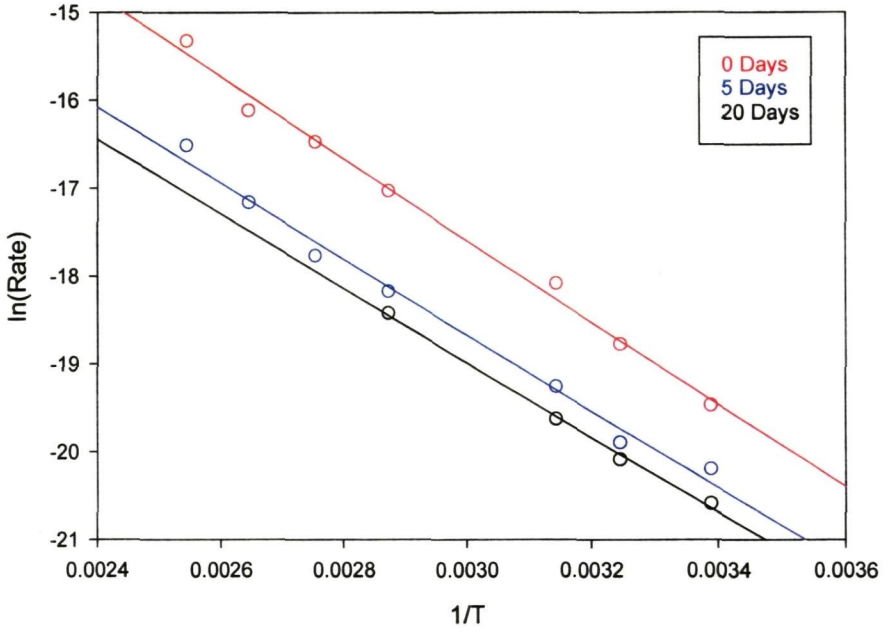

Figure 3.9. Arrhenius plots for -32 mm Puxtrees coal

The data in this plot are for the –32 mm full range material but the same trend was found for all other particle size fractions. The rates shown in Figure 3.9 were measured at periods of between 0 and 20 days from the commencement of each experiment with the initial rates determined by extrapolating the rate curve back to $t = 0$. Initial rate data are important because they represent the rate when it is under purely chemical control since at $t = 0$ there is not yet any product layer formed on the coal surface which can provide diffusive resistance.

The activation energies calculated from these plots and pre-exponential factors are shown in Table 3.4. The errors associated with these values (estimated by least squares analyses) are also shown in Table 3.4. This range of activation energies is consistent with other work

where values between about 10 to 70 kJ/mol have been reported (e.g. Carpenter and Giddings, 1964; Nordon *et al.*, 1979; Karsner and Perlmutter, 1981; Kaji *et al.*, 1985).

There was a slight decrease in activation energy with increasing time, varying from about 39 kJ/mol at *t=0* to 35 kJ/mol at *t=20* days. Although there are rather high errors associated with the pre-exponential factors (since these were calculated from the intercept of a logarithmic plot) they also appeared to decrease from about 0.027 to 0.002 kg O_2 kg $coal^{-1}$ s^{-1} over the same period.

Table 3.4. Activation energies and pre-exponential factors at different times for –32 mm Puxtrees coal

Time (days)	*Activation Energy (kJ mol^{-1})*	*Pre-exponential Factor (kg O_2 kg $coal^{-1}$ s^{-1})*
0	38.8 ± 1.4	2.68×10^{-2} $+1.77 \times 10^{-2}$, -1.07×10^{-2}
2	37.0 ± 2.5	7.29×10^{-3} $+1.05 \times 10^{-3}$, -4.30×10^{-3}
5	36.0 ± 1.6	3.37×10^{-3} $+2.61 \times 10^{-3}$, -1.47×10^{-3}
10	36.2 ± 1.6	4.64×10^{-3} $+3.43 \times 10^{-3}$, -1.97×10^{-3}
20	35.3 ± 1.3	1.90×10^{-3} $+1.21 \times 10^{-3}$, -7.40×10^{-4}

The reduction in activation energy is probably a consequence of the rate controlling mechanism changing with respect to time. At the beginning of the reaction, the rate is controlled purely by the intrinsic rate of reaction, however, as the reaction front moves deeper into the coal particles, diffusive resistances begin to have an effect and tend to limit the flow of oxygen to the reaction surfaces.

The decrease in the pre-exponential factor is consistent with the concept of this parameter representing the number of active sites on the coal surface. A decrease in the pre-exponential factor implies a reduction in the available sites as they are progressively consumed by the reaction.

The activation energies determined for the individual particle size fractions were similar in magnitude ranging from about 36 to 55 kJ/mol with an average of about 45 kJ/mol. There

was a slight trend of decreasing activation energy with increasing particle size (Figure 3.10) which agrees with the findings of Akgün and Arisoy, 1994. Decreasing activation energy with increasing particle size suggests that the overall rate controlling step in the oxidation reaction tends to diffusion at larger particle diameters.

The activation energy measured for the full range material was towards the low end of the range determined for the individual fraction because most of this material comprised particles larger than 9 mm (see Table 4.1 in Chapter 4).

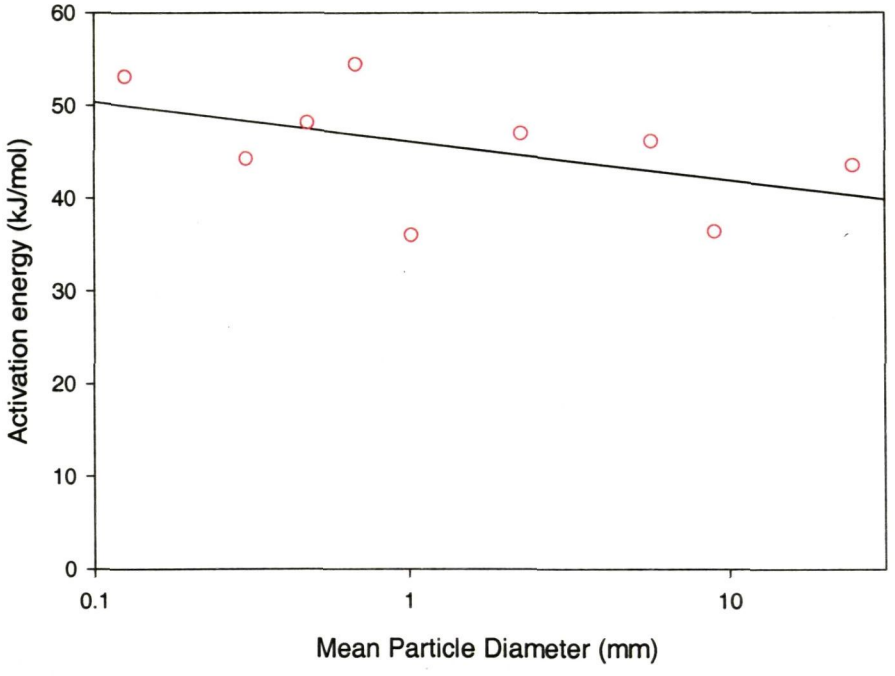

Figure 3.10. The dependence of apparent activation energy on particle size

3.2.3 Effect of Coal Petrology

Vitrinites are by definition macerals which have been protected from oxidation during coal formation, so they would expected to be intrinsically more reactive than inertinites which have been exposed to oxygen. This is supported by the work of various authors (e.g. Davidson, 1990) who have found evidence to indicate that vitrinites are more extensively oxidised at low temperatures than inertinites. Nandi *et al.*, 1977, also found that inertinites

were less reactive under high temperature combustion conditions. Accordingly, it was considered possible that the vitrinite enriched fine fractions of the Puxtrees sample may be inherently more reactive than the large particle diameter vitrinite depleted material.

To test this hypothesis, a sample of the 8-10 mm coal was crushed to less than 250 μm. The rate of oxidation of this crushed material was then measured at 90 °C and compared to that of the original -250 μm fraction. Figure 3.11 shows the results of this experiment.

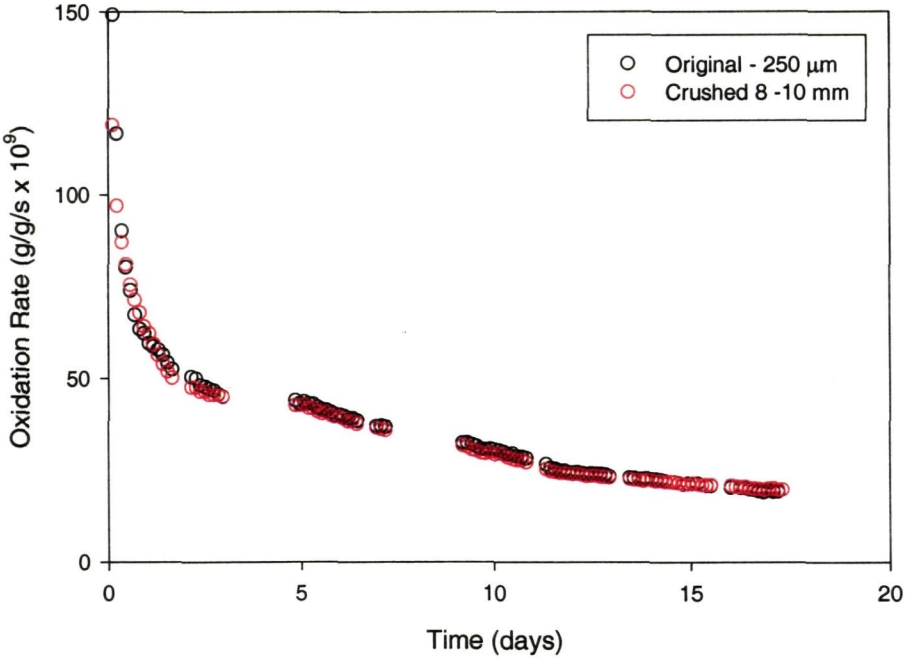

Figure 3.11. Comparison of oxidation rate curves for 8-10 mm which had been crushed to -250 μm and the original -250 μm fraction

The original -250 μm sample had a vitrinite content more than 50 percent greater than the crushed 8-10 mm material (Table 3.2), yet the oxidation rates of the two samples were virtually identical. This is surprising and suggests that there is little difference in the reactivity of the various macerals in this coal. It could also be that the apparently higher surface area of the inertinite offsets any reduced reactivity relative to vitrinites so that the overall rate is about the same. Whatever the reason, the result of this experiment show that, for this coal, the observed reduction in oxidation rate with increased particle diameter is

not due to differences in maceral composition. For other coals, however, this may not be the case.

3.2.4 Effect of Particle Size

Figure 3.12 shows the oxidation rate measured at 120 °C as a function of time for several particle size ranges. In this example, the rate was highest for the fine particles and lowest in the largest. At 14 days, when the measurements were stopped, the rate of the <250 μm material was more than twice that of the 8-10 mm sample.

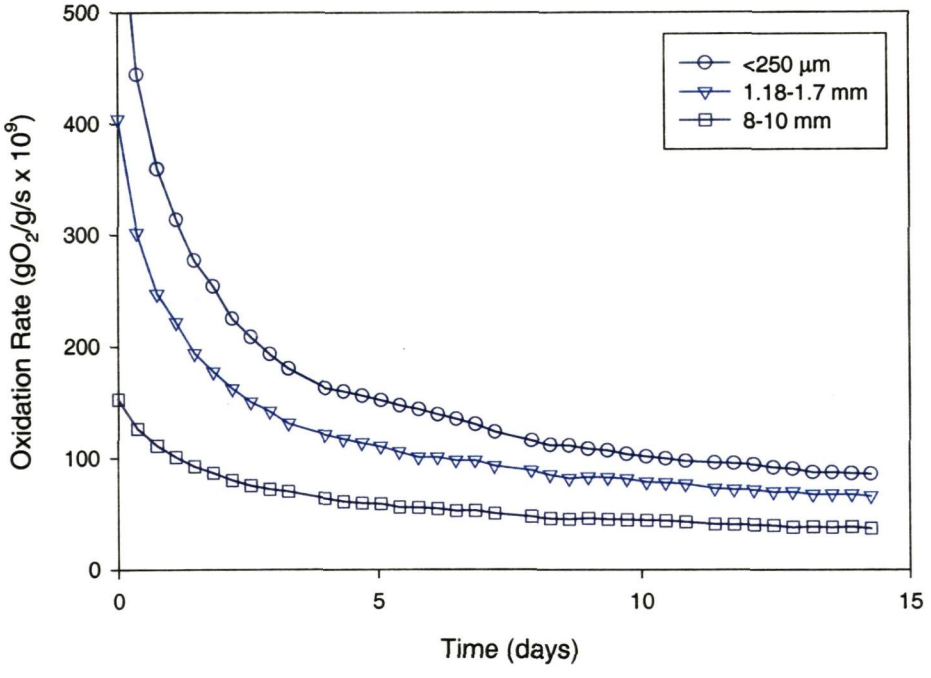

Figure 3.12. The dependence of oxidation rate (at 120 °C) on particle size

At 75 °C, the shapes of the rate curves were similar (Figure 3.13) but they tended to converge so that after a few days the difference in rate between the finest and coarsest particles was only slight. After 14 days the rate of oxidation at 75 °C of the <250 μm material was only about six percent higher than the 8-10 mm particles.

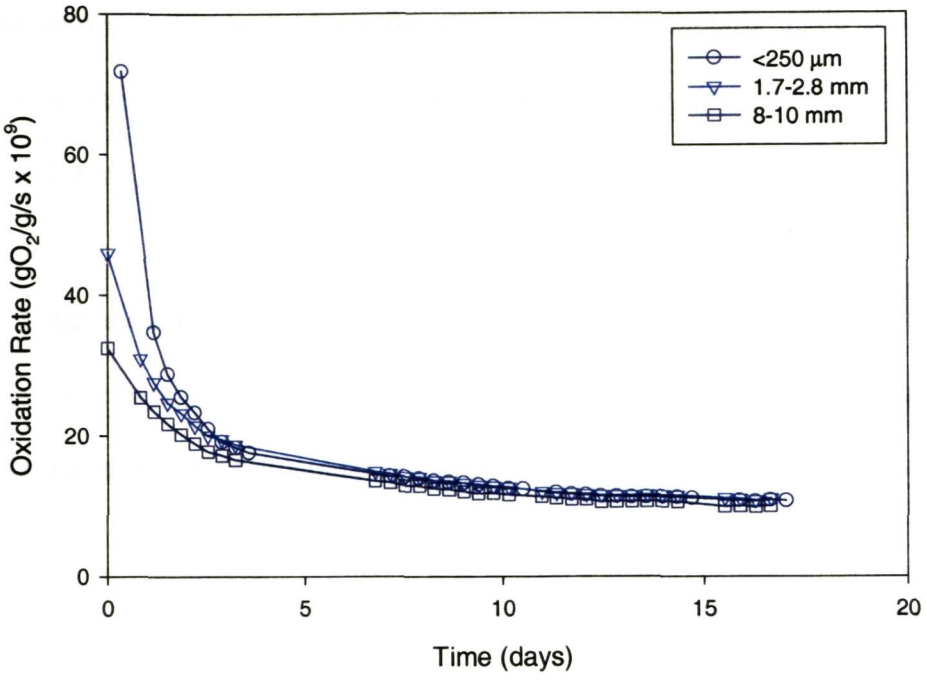

Figure 3.13. The dependence of oxidation rate (at 75 °C) on particle size

The effect of particle size is seen more clearly when the logarithm of the oxidation rate at a particular time is plotted against the logarithm of the mean particle diameter (Figure 3.14).

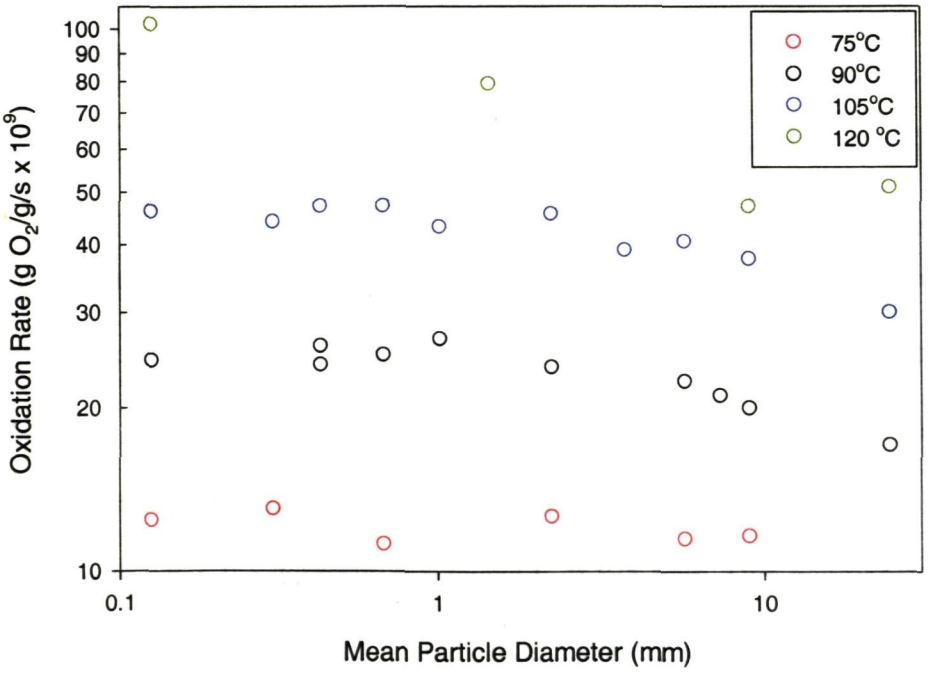

Figure 3.14. The dependence of oxidation rate (measured at 10 days) on particle size

The data shown in Figure 3.14 are based on rate measurements made at 10 days. The shape of the curves, however, was the same when rates determined at other times were plotted in this way.

At 75 °C, the rate seemed to be virtually independent of particle size although there was a very slight decrease with increasing particle diameter. At higher temperatures, however, the effect was much more pronounced and was not linear over the full particle size range.

The results for 90 and 105 °C show a region corresponding to a particle diameter below about 1 mm where the oxidation rate was independent of particle size. Beyond this range, the rate decreased with increasing particle diameter. In the case of the 75 °C data, the rate appeared to decrease very slightly over the entire particle size range, however, this is possibly a consequence of the scatter in the experimental results which may be obscuring the true shape of the curve. It is likely that there is a similar region where the rate is not affected by the particle size. At 120 °C, the oxidation rate decreased with increasing particle size over the entire particle size range.

In the region where the rate decreased with particle size, the increase in rate with decreasing particle diameter was not due to the change in surface area exposed by crushing the particles to smaller sizes. This increase in external area is trivial compared to the internal area of the coal. For example, particles with a mean diameter of 7.35 mm have an external surface area (assuming spherical geometry) of 6.28×10^{-4} m^2/g which increases to 3.69×10^{-2} m^2/g when the diameter is reduced to 0.125 mm. This compares to an internal area determined by CO_2 adsorption of more than 150 m^2/g for both particle sizes. Thus, the observed changes in rate are more likely to be a consequence of the rate at which oxygen can access this internal area.

In the regions where the overall oxidation rate was not affected by particle size, the chemical rate of reaction was apparently low enough so that the rate of diffusion of oxygen into the pore network was sufficient to keep pace with the rate at which it was consumed by the coal. At higher temperatures, however, where the chemical rate is faster, oxygen is consumed faster and the rate of diffusion of oxygen to the reaction surface is no longer high enough to supply the required oxygen to maintain the reaction under purely chemical control. In this situation the overall process becomes diffusion limited.

A number of groups who have investigated the effect of particle size on the rate of oxidation have noted an empirical relationship between rate and particle diameter of the form:

$$R_O \propto d^{-m} \qquad (3.1)$$

where R_O is the rate of oxidation at a given time, d is the particle diameter and m is an exponent specific to the coal and experimental conditions. A plot of $log(R_O)$ versus $log(d)$ will yield a straight line with a slope of $-m$.

The values of m for the particle size dependent regions in the current study were evaluated for each temperature and were found to increase from 0.04 at 75 °C to 0.23 at 120 °C. In the regions where there was no particle size effect, the value of m was zero. On the basis of the rationale proposed by Akgün and Arisoy, 1994, (described in Chapter 1) the oxidation rate of this coal is under purely chemical control at particle sizes less than about 1 mm diameter. As well, at temperatures below about 75 °C, the rate is also essentially determined by the intrinsic chemical rate of reaction.

At higher temperatures and at particle sizes above 1 mm, diffusive effects start to become important so that the overall rate in these regions is increasingly determined by the rate at

which oxygen can diffuse to the reaction sites within the particles. The increase in *m* with increasing temperature shows that diffusive resistance is increasing as the rate of chemical reaction increases.

Compared to other coals, the Puxtrees sample used in the current work appears to be relatively porous because the values of the exponent, *m*, are relatively low. The mercury porosimetry measurements made on this coal also indicated that it is relatively porous in nature. In Akgün and Arisoy's 1994 study, they examined a Turkish lignite and found that the rate at 75 °C was strongly influenced by the particle diameter and evaluated *m* as 0.74 under their experimental conditions. In another fairly recent study, Pànek and Taraba, 1996, examined a large number of bituminous and sub-bituminous coals and, in the regions where there was particle size dependence, *m* was in the range of 0.3 to 0.45. The temperature of their experiments was 30 °C so presumably at higher temperatures, even higher values of *m* would have been found.

Bainbridge and Szemes (unpublished results) also examined the effect of particle size on oxidation rate. They measured the rate at 75 °C for a Hunter Valley coal (from the St Helliers seam) of five fractions with mean particle diameters ranging from 0.75 to 16 mm. They found that under these conditions, the rate decreased significantly with increasing particle size but unlike the Puxtrees sample used in this study, there was no region where the rate was not affected by particle size. The value of *m* calculated from these data was 0.17. This is a much higher value than that determined for the Puxtrees sample at 75 °C indicating that diffusion was controlling the rate more strongly than in the Puxtrees probably because the coal was less porous. The fact that these workers did not find a region where the rate was not affected by the particle size also suggests that the coal was

less porous. It is likely, however, that had they made measurements on sufficiently small fractions, such a region would have been observed.

When the oxidation reaction is under purely chemical control, the rate is determined by the amount of surface in contact with oxygen. Thus, if the intrinsic reactivity of the coal is the same across all of the particle sizes, the oxidation rate (per g of coal) divided by this surface area (per g of coal) should be a constant across the entire particle size range at a given temperature. The chemical composition of this sample of Puxtrees coal was the same for all of the size fractions and the differences in petrology were found to have no effect on the rate. Hence it can be reasonably assumed that the reactivity of the coal was the same for all particles.

To estimate the surface area of coal reacting, it is tempting to assume that all particles are spheres and calculate the external surface area based on spherical geometry. In fact, this is usually the basis of any model that attempts to include the effect of particle size. However, when rate data are divided by the areas calculated on this assumption, the resultant normalised rates increase sharply with increasing particle diameter. Figure 3.15 illustrates the effect when rate data measured at 90 ^{o}C were normalised to the spherical external surface areas calculated from the mean particle diameter for each fraction. In this case, the normalised rate increased over two orders of magnitude.

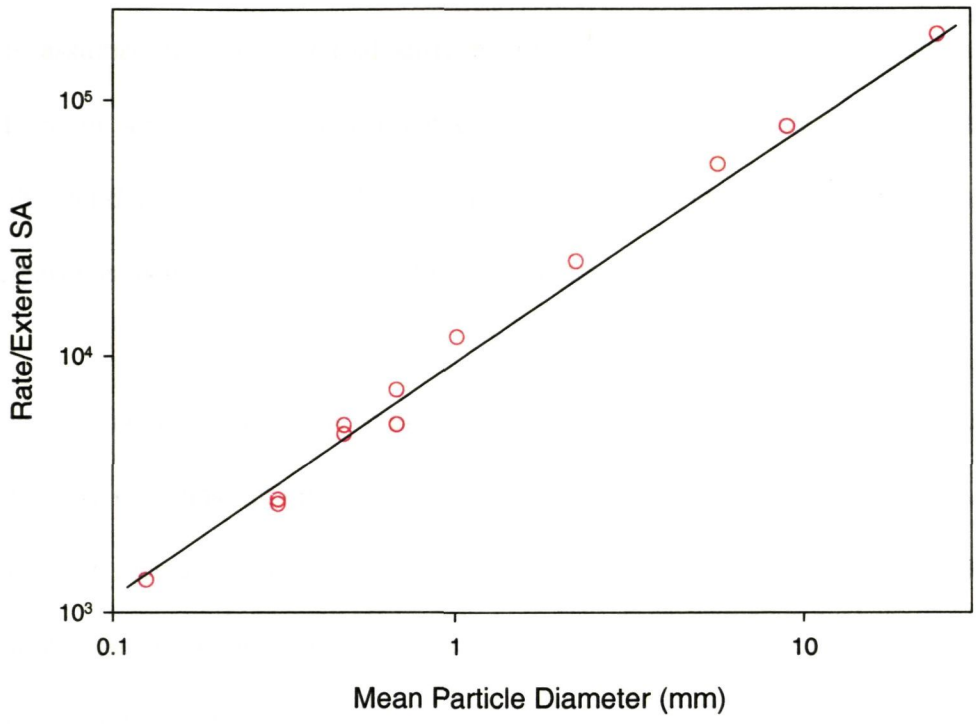

Figure 3.15. Oxidation rate at 90 °C normalised to the spherical external surface area

This is showing that the surface available for reaction is greatly underestimated by assuming that this surface is simply the surface of a solid sphere.

Even a cursory examination of the coal samples reveals that the particles are not really spherical but are actually irregular and angular in shape. To estimate the true external surface area of the particles, some of the larger particles were measured directly. The surfaces of several particles from each the 4.75-6.0, 8-10 and 16-32 mm fractions were traced onto graph paper and the squares counted to estimate their respective areas.

The results of these estimates are compared to the spherical surface areas in Table 3.5.

Table 3.5. Comparison of measured and calculated external surface areas

Particle Size Range (mm)	*Measured Area (m^2/g)*	*Spherical Area (m^2/g)*
4.75-6.7	1.86×10^{-3}	9.12×10^{-4}
8-10	8.78×10^{-4}	5.59×10^{-4}
16-32	4.14×10^{-4}	2.59×10^{-4}

The actual area is about 60-100 percent higher than that calculated by spherical geometry. If it is assumed that the external surface areas are on average 80 percent higher than calculated by simple spherical geometry and the rates divided by this corrected surface area, the trend shown in Figure 3.13 is still apparent. Obviously, the external surface area of the particles is not representative of the actual area of the coal in contact with oxygen.

The surface area available for reaction is clearly not the entire internal surface area measured by CO_2 adsorption. If it were, the measured rates for this coal would actually increase with increasing particle diameter since the highest surface areas were measured on the largest particles. As discussed previously, the relatively high CO_2 surface areas reported for coal (compared to nitrogen, for example) may be partly a consequence of the high solubility of this gas in coal which allows it to enter "blind" pores. These pores are not accessible to mercury or helium and so are probably not accessible to oxygen either. It is likely then that oxygen penetration, in the initial stages of reaction at least, is confined to a region close to the external surface of the particle. The depth of penetration would depend on the extent to which the fissure structure of the particle was developed.

Mercury porosimetry measurements showed that the volume of pores greater than 3.75 nm in diameter (i.e. the macroporosity) decreased with increasing particle diameter so it was thought that this may be a function of the true reactive surface area. Replotting the 90 °C data shown in Figure 3.15, but using the total intruded volume instead of external spherical surface area, yielded Figure 3.16.

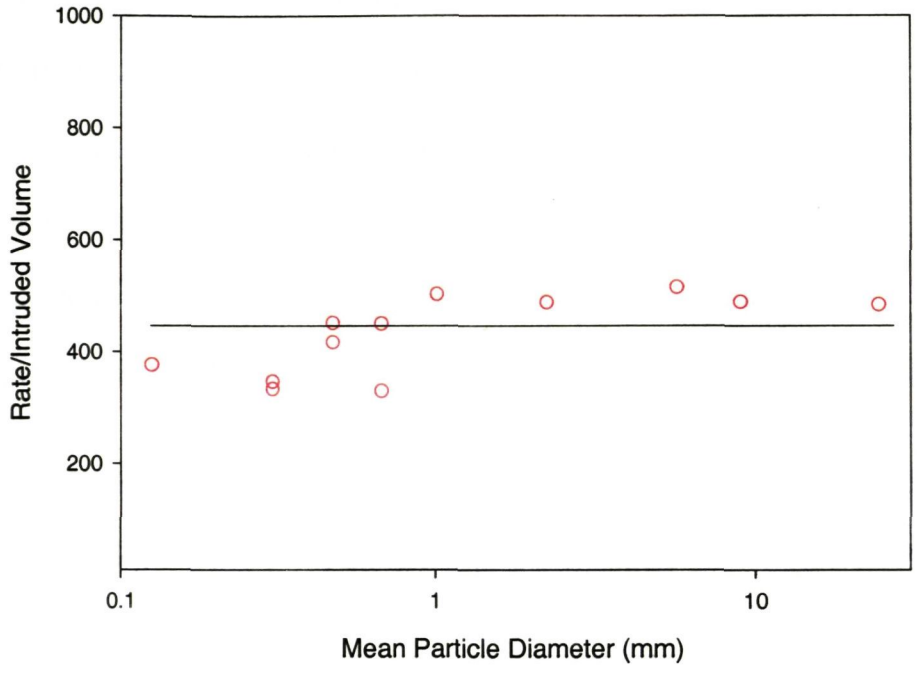

Figure 3.16. Oxidation rate at 90 °C normalised to the mercury intruded volume

Here, the normalised rate is almost constant over the full particle size range. It is important to note here that the surface of the macropores, which can be calculated from the intruded volume, is not necessarily a direct measure of the reactive surface. In this case, it is not since the surface area of these pores was about 10 m^2/g for all of the particles. Rather, it is a measure of the accessibility of oxygen to the micropores where most of the reactive surface resides.

These results show that the rate of oxidation of the coal is determined by (all other things being equal) the macro-porosity of the material and that the mean particle diameter, *per se*, is not necessarily related to the overall reactivity. The intruded volume appears to provide an indirect measure of the accessibility of the coal's internal reactive sites to oxygen.

3.3 References

Allardice, D. J., *Carbon*, 1966, **4**, 255-262

Carpenter, D. L. and Giddings, D. G., *Fuel*, 1964, **43**, 247-266.

Carras, J. N. and Young, B. C., *Prog. Energy Combust. Sci.*, 1994, **20**, 1-15.

Chen, X. D. and Stott, J. B., *Combustion and Flame*, 1997, **109**, 578-586.

Hill, C. R., MSc Thesis University of Witwatersrand, 1986

Kam, A. Y., Hixson, A. N. and Perlmutter, D. D., *Chem. Eng. Sci.*, 1976, **31**, 815.

Karsner, G. G. and Perlmutter, D. D., *AIChE*, 1981, **27**, 920-926.

Keleman, S. R. and Freund, H., *Enegy and Fuels*, 1990, **4**, 165-171.

Killingley, J. S. in *Methane Drainage From Coal,* Paterson, L., Ed.; CSIRO Australia, 1990

Larsen, J. W., Hall, P. and Wernett, P. C., *Energy and Fuels*, 1995, **9**, 234-330.

Monazam, E. R., Shadle, L. J., Evans, R. and Schroeder, K. *Energy and Fuels* 1998, **12**, 1299-1304

Nandi, B. N., Brown, T. D. and Lee, G. K., *Fuel*, 1977, **56**, 125-130.

Palmer, A. D., Cheng, M., Goulet, J. C. and Furimsky, E., *Fuel*, 1990, **69**, 183-188.

Pànek, P. and Taraba, B., Coal and its interaction with oxygen Ostravskè Univerzity, Monograph 92, 1996

Sondreal, E. A. and Ellman, R. C., Laboratory determination of factors affecting storage of North Dakota lignite, US Bureau of Mines Report of Investigation No 7887, 1974

Smyth, M. in *Methane Drainage From Coal,* Paterson, L., Ed.; CSIRO Australia, 1990

Stach, E., Mackowsky, M.-Th., Teichmüller, M., Taylor, G. H., Chandra, D. and Teichmüller, R., in Coal Petrology, Gebrüder Borntraeger, Berlin, Stuttgart 1982, pp 45.

Standards Association of Australia. *Australia Standard AS 1038: Methods for the analysis and testing og coal and coke Part 2 – Forms of sulphur in coal.* Standards Association of Australia, Sydney, 1973

Standards Association of Australia. *Australia Standard AS 1038.3: Coal and coke – analysis and testing Part 3: Proximate analysis of higher rank coal.* Standards Association of Australia, Sydney, 2000

Standards Association of Australia. *Australia Standard AS 1038.6.1: Coal and coke – analysis and testing Part 6.1: Higher rank coal and coke – Ultimate analysis – Carbon and hydrogen.* Standards Association of Australia, Sydney, 1997

Standards Association of Australia. *Australia Standard AS 1038.6.2: Coal and coke – analysis and testing Part 6.2: Higher rank coal and coke – Ultimate analysis – Nitrogen.* Standards Association of Australia, Sydney, 1997

Wang, H., Dlugogorski, B. Z. and Kennedy, E. M. *Energy and Fuels* 1999, **13**, 1173-1179

Chapter 4

Modelling of Oxidation Kinetics

4.1 Introduction

A goal of many investigations of low temperature coal oxidation has been to develop a general model which can predict temperatures within piles of coal or mine waste and various models have been proposed which attempt to estimate the temperature profiles of piles of given geometries. These models are complex and usually require numerical methods for their solution. To be successful, any model must include reliable mathematical representations of all of the heat generation and heat loss mechanisms at work in the coal or waste pile. Since low temperature oxidation is the main source of heat, it is essential that these models include a component which can accurately predict the rate of oxidation of the coal. For this reason, a considerable amount of effort has been directed for more than half a century towards formulating an oxidation rate model for coal.

One aspect of kinetic modelling where there has been almost universal agreement is the effect of temperature. Virtually all studies of low temperature oxidation kinetics, in which the effect of temperature has been examined, report a temperature dependence which obeys an Arrhenius like relationship. For the Puxtrees coal, the Arrhenius equation was applicable over the temperature range of 22 to120 ^{o}C (see Effect of Temperature in Chapter 3). As noted in Chapter 3, the activation energy and pre-exponential factor (Table 3.4) decreased slightly with time. The data from Table 3.4 have been plotted in Figures 4.1 and 4.2 and show the effect of time on the activation energy and pre-exponential factor respectively.

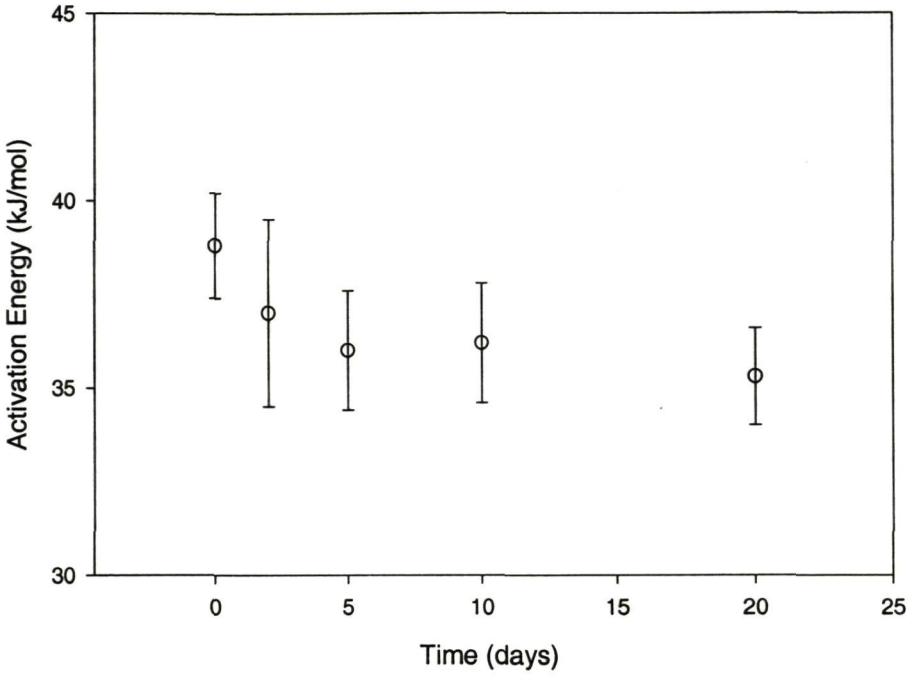

Figure 4.1. The dependence of activation energy on time

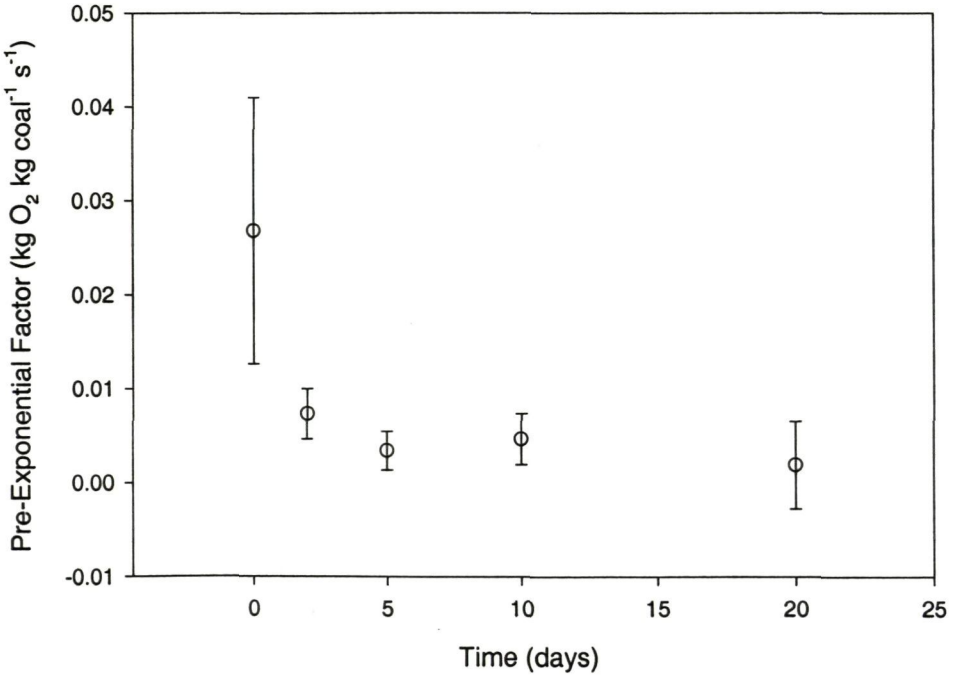

Figure 4.2. The dependence of pre-exponential factor on time

It would be possible to fit a curve to these data and thus establish empirical expressions for the activation energy and pre-exponential factor as a function of time. Similarly, particle size effects could be modelled by plotting the kinetic parameters against particle size (see Figure 3.10, for example). In principle then, this would provide a model of the oxidation kinetics of Puxtrees coal which could predict the rate as a function of temperature, time and particle size. However, apart from the Arrhenius component, it would be purely empirical and as such provides no insight into the underlying mechanisms of the reaction.

The remaining part of this chapter is devoted to examining several, increasingly sophisticated, kinetic models which have been proposed for low temperature oxidation of coal. The first of these is the Elovich equation, which is a simple, empirical model that has its origins in studies of chemisorption of gases onto solids but, despite some shortcomings, has been widely applied to coal oxidation kinetics.

The second model to be examined is the shrinking core model which is a more sophisticated model than the Elovich equation and has the advantage that the chemical rate constant, diffusivity and particle size are all specifically included in the model. Despite the apparent advantage of this model over the more popular Elovich equation, it has not been widely used in relation to low temperature coal oxidation.

Recently, a quite complex rate model, the pore tree model, was applied to low temperature coal oxidation kinetics (Wang *et al.*, 1999). This model was developed to take into account the porous structure of coal and results of modelling performed by Wang *et al.* suggested that it successfully simulated observed particle size effects. However, these authors did not directly compare the their model results with measured oxidation rates.

In the following sections, the results of the rate measurements made on Puxtrees coal are compared to the Elovich, shrinking core and pore tree models.

4.2 The Elovich Model

As has already been shown in this and many other studies, the rate of low temperature oxidation of coal decreases with time. To describe this time-dependent kinetic behaviour, many authors (e.g. Allardice, 1966; Nordon *et al.*, 1979; Kaji *et al.*, 1987; Khan *et al.*, 1990; Akgün and Arisoy, 1994; Pánek and Taraba, 1996; Teng and Hsieh, 1999) have used the Elovich equation.

In the 1930s, Roginsky and Zeldovich, 1934, and Elovich and Zhabrova, 1939, developed a simple empirical expression to model the rate of chemisorption of gases onto solids, R_a, at constant temperature and pressure:

$$R_a = ae^{-\alpha\theta} \tag{4.1}$$

where θ is the fraction of active sites occupied and a and α are constants. If θ is replaced by the amount of reactant adsorbed, q, then Equation 4.1 can be written as:

$$R_a = \frac{dq}{dt} = ae^{-\alpha q} \tag{4.2}$$

This expression has come to be known as the Elovich equation and can be integrated to give:

$$q = \frac{1}{\alpha}\ln(t + \frac{1}{a\alpha}) - \frac{1}{\alpha}\ln(\frac{1}{a\alpha}) \tag{4.3}$$

At the suggestion of Taylor and Thon, 1952, $\frac{1}{a\alpha}$ is often replaced by t_0 so that Equation 4.3 can be rewritten as:

$$q = \frac{1}{\alpha}\ln(t + t_0) - \frac{1}{\alpha}\ln(t_0) \tag{4.4}$$

This equation can be tested against experimental data by plotting q against $ln(t + t_0)$. With a suitably chosen value of t_0, a straight line is obtained with a slope of $1/\alpha$ if Elovich kinetics apply. The value of a is calculated from:

$$a = 1/t_0\alpha \qquad (4.5)$$

Although some authors (e.g. Taylor and Thon, 1952) have attempted to establish the physical significance of the Elovich parameters a, α and t_0, others (e.g. Nordon *et al.*, 1979; Carras and Young, 1994) accept that, at least in relation to low temperature oxidation of coal, they are empirical curve-fitting constants.

The purpose of the term t_0 is to linearise the plot of q against $ln(t + t_0)$. If this parameter is not used or the value chosen is too low or too high, the plot is almost always markedly curved at its beginning. The curvature of the plot implies that there is another, faster, adsorption process at work simultaneously in the initial stages of adsorption. This is usually confirmed by the fact that the initial rate (which corresponds to a when $q = 0$) calculated from Equation 4.2 is usually somewhat lower than the observed rate at $t = 0$.

Figure 4.3 illustrates this point by comparing the measured oxidation rate of Puxtrees coal in air at 90 °C with the corresponding Elovich model. In this example the calculated initial rate is 55 x 10^{-9} g O_2/g/s compared to the observed rate of about 90 x 10^{-9}g O_2/g/s. Notice, however, that the model fits the experimental data quite well during the later stages of adsorption. This good fit is often observed and is the reason for the widespread use of the Elovich model in coal oxidation studies.

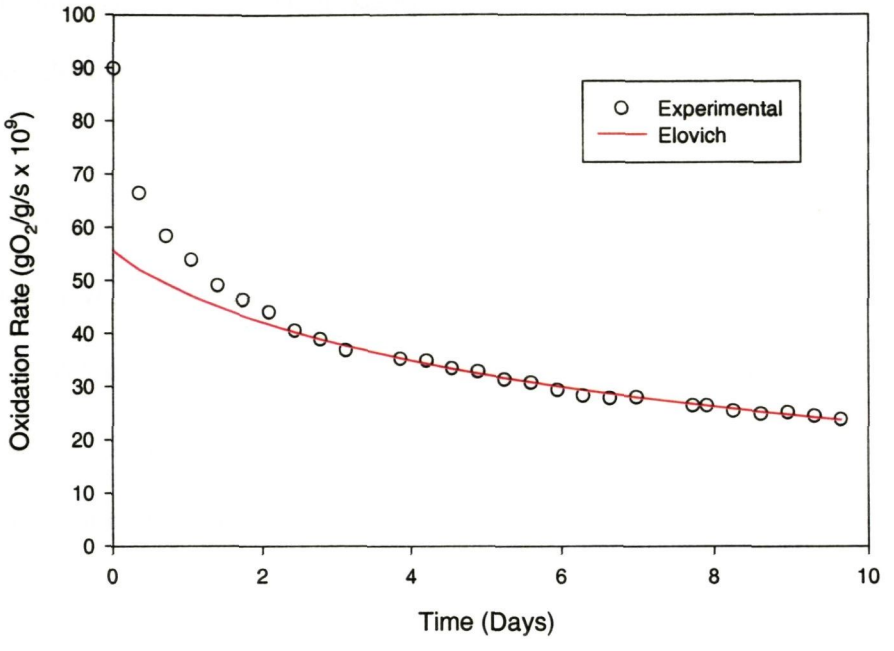

Figure 4.3. Comparison of Elovich model with experimental data for Puxtrees coal at 90 °C. The particle size was 1.7-2.8 mm.

The value of t_0 is often chosen simply by trial and error until the "best", i.e. most linear, plot of q versus $ln(t + t_0)$ is obtained. Aharoni and Ungarish, 1976, developed a more quantitative approach in which they took account of the fact that Elovich kinetics only commence after a finite time. Their method involves plotting t against the reciprocal of the rate, $(dq/dt)^{-1}$, Z, according to the expression:

$$t = Z / \alpha - t_0 \qquad (4.6)$$

The slope of this plot yields α and by extrapolating to $Z = 0$, t_0 is obtained.

Taylor and Thon, 1952, accounted for the discrepancy between observed and calculated initial rates in terms of an "initial massive adsorption" which they assumed to be occurring as $t \rightarrow 0$ thus assigning a virtually infinite rate to the process. The idea of an initial fast reaction which precedes the Elovich kinetics is consistent with the findings of Pànek and Taraba, 1996, who, using a calorimetric technique, claimed to be able to measure separately the rates of physical adsorption and chemical reaction of oxygen by coal. They

found that the rate of physical adsorption > the rate of chemical interaction > the rate of oxygen diffusion into the coal.

The Elovich model does not include the effects of either particle size or temperature. Nordon *et al.*, 1979, extended the equation to take account of temperature by combining it with the Arrhenius equation. A further development of the extended model of Nordon *et al.* was made by Bernaudat, 1999, who established an empirical relationship between the oxidation rate and carbon content of carbonaceous materials dumped during coal mining operations. So far, however, there has not been a combined model which effectively takes account of the particle size.

4.2.1 Results

The results from this study were processed using the method of Aharoni and Ungarish, 1976, to evaluate the Elovich parameters for all of the oxidation experiments. For each condition of particle size and temperature, the values of a and α were determined and the resultant Elovich curve compared to the experimental data. In general, the results were similar to those illustrated in Figure 4.3 which shows the results for 2.25 mm particles at 90 °C. The model usually provided quite a good fit to the experimental data for times greater than about three to four days, but the initial rate was always substantially underestimated.

Since a is effectively the rate at $t=0$, it was found to increase with increasing temperature and decreasing particle size in the same way as shown in the experimental data (Figure 4.4). The a parameter, not surprisingly perhaps, followed the Arrhenius relationship and yielded an average activation energy of approximately 55 kJ/mol, which compared reasonably well to the average value of around 45 kJ/mol measured directly from the experimental data.

The effect of temperature and particle size on α was rather different. In this case there was no particle size effect but the value decreased with increasing temperature according to a linear relationship with a slope of -0.773 and an intercept of 99.4 with a high correlation coefficient of 0.9888 (Figure 4.5).

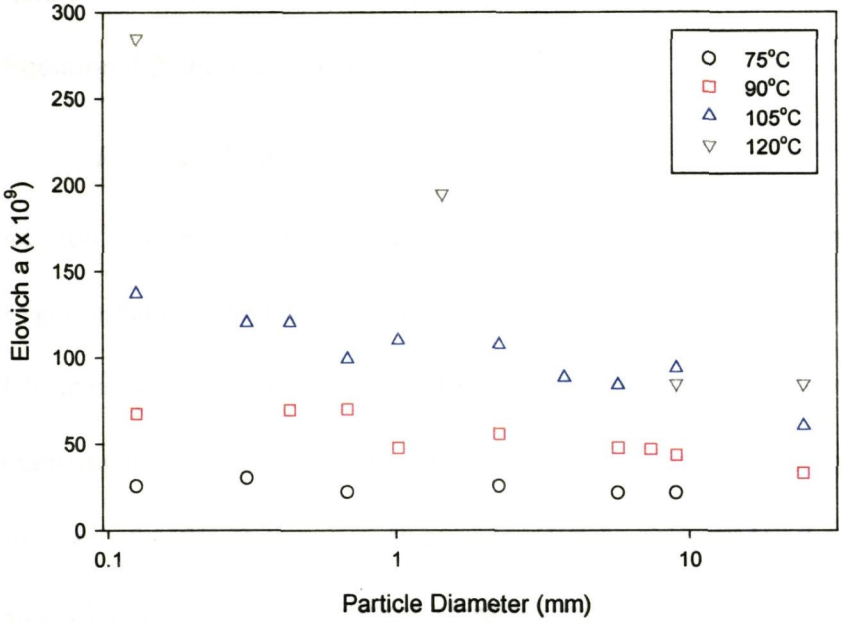

Figure 4.4. The dependence of the Elovich *a* parameter on particle size

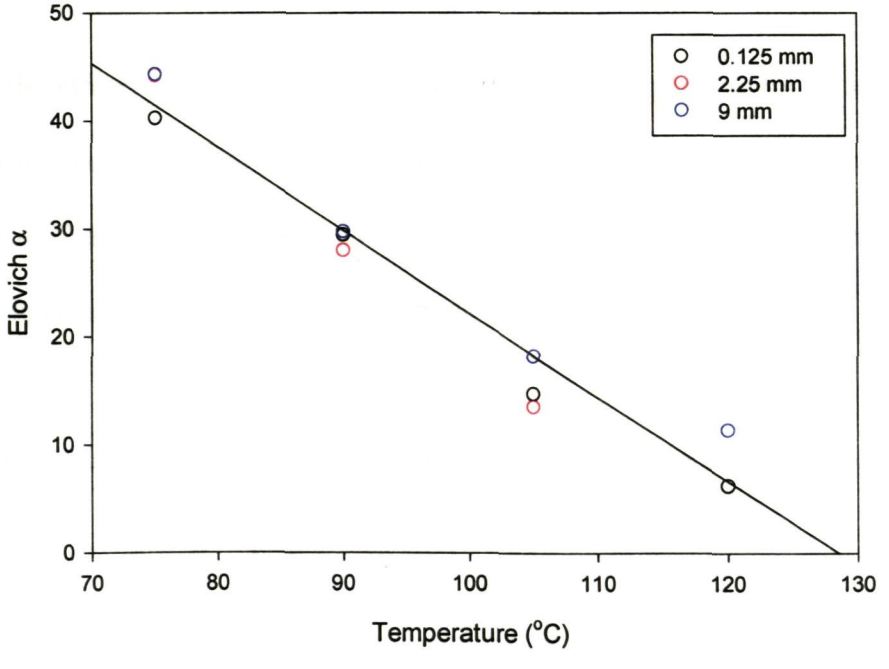

Figure 4.5. The dependence of the Elovich α parameter temperature

These results show that both the Elovich a and α parameters are functions of temperature:

$$a = Ae^{-\frac{E}{RT}} \tag{4.7}$$

and

$$\alpha = c - bT \tag{4.8}$$

where b and c are the slope and intercept respectively. By substituting Equations 4.7 and 4.8 into Equation 4.2, the Elovich equation becomes:

$$R_O = Ae^{-E/RT}e^{-(c-bT)q} \tag{4.9}$$

This expression enables the rate of oxidation to be calculated for any time (i.e. determined by the oxygen uptake, q) and temperature and is very similar to that developed by Nordon *et al.*, 1979, and used later by Bernaudat, 1999. It cannot, however, account for changes in particle diameter so a and α must be evaluated for each particle size or a given particle size range. However, for the Puxtrees coal sample used in this study, there was very little particle size effect at temperatures below about 75 °C. Therefore the effect of particle size can be neglected at low temperatures for this coal.

To test the effectiveness the Elovich model, the various parameters of activation energy, pre-exponential factor and c and b were substituted into Equation 4.9 to calculate rate curves for 22 and 35 °C. These curves were then compared to the actual rates measured at these temperatures for the –32 mm full range material.

Figure 4.6 compares the measured rates at 22 and 35 °C to the modelled rates.

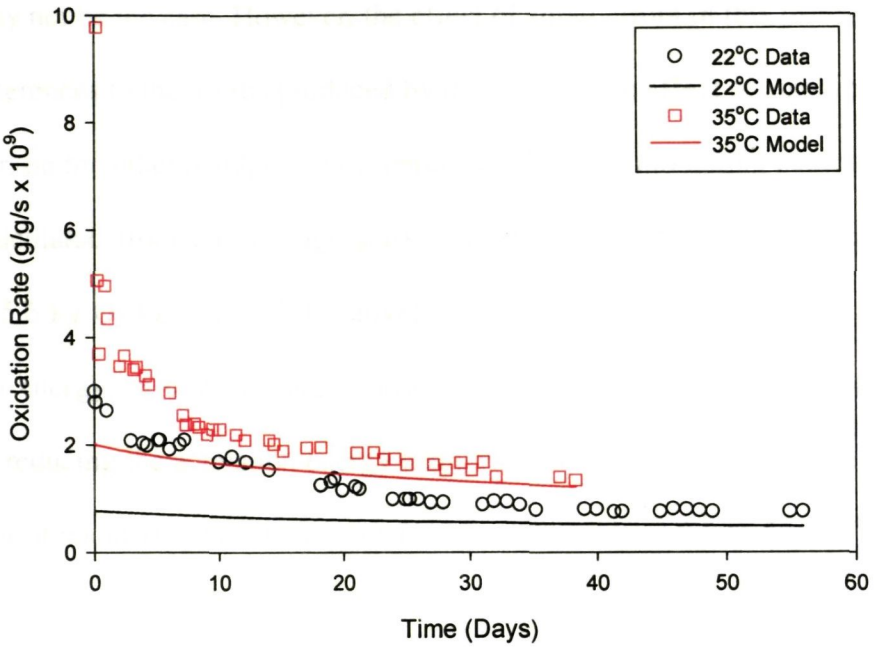

Figure 4.6 Comparison of measured oxidation rates at 22 and 35 °C to those predicted by the Elovich model

In both of the examples shown in Figure 4.6 the Elovich model has substantially underestimated the oxidation rate. For the 35 °C case, the rate predicted by the model is less than half the measured rate at $t = 0$ and at 22 °C, the difference between measured and predicted is even greater. At greater times, the measured and modelled rates tend to converge so that after about 30 days, the modelled and measured rates at 35 °C are about the same. At 22 °C, however, the modelled rate is still less than the measured rate even after 50 days.

Although Equation 4.9 can in principle be used to estimate the rate of reaction as a function of time, it is apparent from the results shown here that the fit is less than satisfactory. The effect of particle size on the oxidation rate is probably not significant for this particular coal at the temperatures considered so the discrepancies between the measured and modelled rates are unlikely to be due to particle size effects. Rather, it is likely that the errors associated with estimating both a and α are large. When estimating α,

it is assumed that relationship in Equation 4.8 holds over the full temperature range, which may not be the case. However, the effect of small errors in this parameter make only slight differences to the results produced by the model. The effect of small changes in the *a* parameter, on the other hand, is very pronounced. For this modelling exercise, the value of *a* was calculated from the average activation energy of 55 kJ/mol and pre-exponential factor of 5.6 kg O_2 kg $coal^{-1}$ s^{-1}. Relatively small changes in these values, particularly the activation energy, resulted in large variations in the rates calculated by the model. For example, reducing the activation energy from 55 to 50 kJ/mol increased the rate calculated by a factor of about 10 (at $t = 0$, the rate increased from about 0.8 to 8 x 10^{-9} g/g O_2/s).

In practical terms the Elovich model does not give a particularly good fit to the measured rates during the initial stages of reaction and because of the errors associated with determining the parameters, its predictive power is of limited value, even when the effects of particle size can be neglected.

4.3 The Shrinking Core Model

4.3.1 Description of the Model

The shrinking core model (SCM) was developed more than 40 years ago (Levenspiel, 1999) to describe the kinetics of certain heterogeneous reactions between a gas (or liquid), A, and a solid, B. In practice, this model it has been found to be applicable to many solid state reactions (Smith, 1970; Levenspiel, 1993).

For the SCM to be applicable, the reaction must be of the form:

$$A(g) + bB(s) \rightarrow R(g) + S(s) \qquad (4.10)$$

and the solid product, S(s), must occupy the same volume as the initial reactant, B(s). This generic reaction is analogous to the low temperature coal-oxygen reaction:

$$O_2 + \text{Coal} \rightarrow CO_2 \text{ and other gaseous products} + \text{oxy-coal} \qquad (4.11)$$

The solid oxy-coal product forms as a layer on the surface of the particles of coal while the reaction proceeds at the surface of an unreacted core which decreases in size with time. This process, for a spherical particle, is illustrated in Figure 4.7.

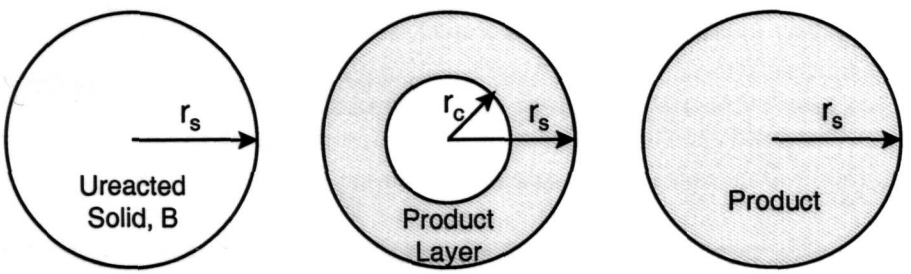

Figure 4.7. Progress of reaction in the shrinking core model (from Denbigh and Turner, 1971)

At $t = 0$, the particle comprises entirely unreacted solid with an external radius of r_s. At $t > 0$, a layer of product has formed on the surface and the unreacted core has shrunk to smaller radius, r_c, although the external diameter of the particle remains unchanged at r_s because the volume of the oxy-coal product and coal are equal. Conversion to product is complete when the radius of the unreacted core reduces to zero.

The rate of the overall reaction may be set by any of several processes which occur in succession. These are:

- diffusion of the reactant gas, oxygen, across a boundary layer from the bulk gas (air) to the external surface of the particle,
- diffusion of oxygen through the product layer to the surface of the unreacted core and
- the chemical reaction between oxygen and coal which occurs on the surface of the core at radius, r_c.

Diffusion through the boundary layer is driven by the difference in concentration of oxygen between the bulk air, C_{Og}, and at the surface of the particle, C_{Os}. Thus the rate is a

function of this concentration gradient but also of the external surface area of the particle, S_s, and the mass transfer coefficient, k_m. Mathematically, this can be written in terms of the number of moles of oxygen being consumed, N_O, per unit time as:

$$-\frac{1}{S_s}\frac{dN_O}{dt} = k_m(C_{Og} - C_{Os}) \tag{4.12}$$

The integrated solution to Equation 4.12 is:

$$t = \frac{\rho_{coal} r_s}{3bk_m C_{Og}}\left(1-\left(\frac{r_c}{r_s}\right)^3\right) \tag{4.13}$$

Diffusion through the boundary layer is generally only a significant resistance at high temperatures where the chemical reaction rate is very high so it is therefore unlikely to be the rate determining step in low temperature coal oxidation. Diffusion through the product layer, on the other hand, may represent a significant resistance to the rate of reaction particularly if the product layer is thick or relatively impervious to the gaseous reactant.

In developing a mathematical expression for the rate of diffusion through the product layer, the so-called steady-state approximation is used. This assumes that at any instant the rate of shrinkage of the unreacted core is slow compared to the movement of oxygen through the pores of the product and so the reaction surface may be considered to be stationary. Using this approach, the diffusive processes are determined for each particle size at a fixed radius then these results are integrated over all values of r (Levenspiel, 1999) to yield:

$$t = \frac{\rho_{coal} r_s^2}{6bD_e C_{Og}}\left\{1-3\left(\frac{r_c}{r_s}\right)^2+2\left(\frac{r_c}{r_s}\right)^3\right\} \tag{4.14}$$

The final potential rate limiting step is the chemical reaction between the components themselves. The rate of the reaction occurring on the surface of a particle is given by:

$$-\frac{1}{S}\frac{dN_O}{dt} = kC_{Og} \tag{4.15}$$

where k is the chemical rate constant. Integration of this expression yields:

$$t = \frac{\rho_{coal}}{bkC_{Og}}\left(r_s - r_c\right) \tag{4.16}$$

The expressions given above form the basis of the shrinking core model and allow the size of the unreacted core to be calculated for any time during the reaction from the initial particle size, bulk gas concentration and density of the solid reactant, all of which are readily measured. The chemical rate constant and effective diffusion coefficient are also required and these too, are measurable physical values but they are somewhat more difficult to measure than the first three noted above.

It can be seen that at the initial condition (i.e. $t = 0$) the reaction is under purely chemical control since there is not yet any product layer. As the reaction proceeds, however, the product layer becomes thicker and it is likely that diffusion will come to control the rate of the reaction. Thus it is unlikely that one process will be rate limiting for the entire reaction but rather a combination of resistances will occur. To account for the combined effects it is simply a matter of adding the times determined in Equations 4.13, 4.14 and 4.16. Since film diffusion can be neglected, the time taken to reach a given unreacted core size is given by:

$$t_{total} = t_{diffusion} + t_{chemical} \tag{4.17}$$

The SCM has an advantage over the Elovich model in that it does not rely on empirical constants but rather is based on measurable physical and chemical properties. As well, it explicitly includes the effect of particle size.

4.3.2 Results

An automated spreadsheet incorporating a Visual Basic routine was used to calculate the global oxidation rate as a function of time from the initial particle size, bulk O_2 concentration and density of the coal, all of which were known quantities. The model also required the chemical rate constant, k, and diffusivity, D_e, to calculate the rate. These parameters were estimated by substituting values for D_e and k into the model and calculating the oxidation rate for each set of conditions of particle size and temperature then comparing the shape of the resultant curve to the experimental data. This process was repeated with different values of D_e and k until the best fit was obtained. The values of D_e and k at the best fit were taken as the "correct" ones.

During this process of trial and error, it was found that the chemical rate constant had most effect on the modelled curve near the beginning of the reaction whereas the diffusivity had little effect early on but became more important during later stages of the reaction. This behaviour demonstrates that the overall rate is changing from chemical control at the start to diffusion control as the thickness of the product layer increases.

A typical curve generated by the model is shown in Figure 4.8.

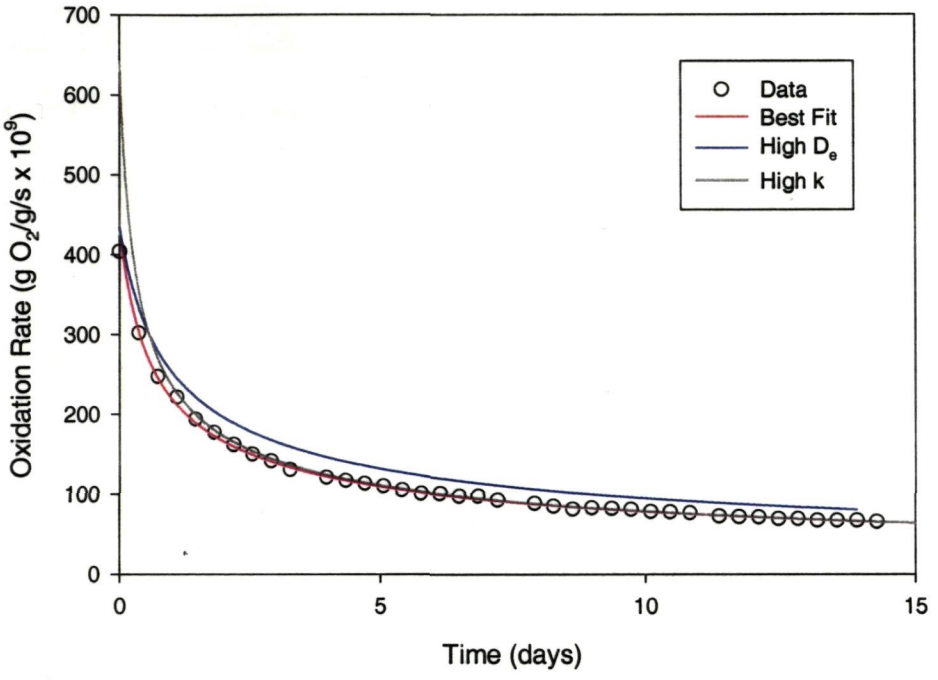

Figure 4.8. Comparison of experimental results for 1.44 mm particles at 120 °C with the SCM calculated curve. The effect of varying k and D_e is also shown – best k = 6.50 x 10^{-5} cm s^{-1}, high k = 9.75 x 10^{-5} cm s^{-1}; best D_e = 1.50 x 10^{-9} cm^2 s^{-1}, high D_e = 2.25 x 10^{-9} cm^2 s^{-1}

This particular example is for coal with a mean particle diameter of 1.44 mm (1.18 to 1.7 mm size range) at 120 °C. The experimental data are shown as open circles with the best-fit curve shown in red. It can be seen that the model has almost perfectly fitted the observed rate for the entire duration of the experiment. Similar very good fits were achieved for most of the other experiments over the entire temperature and particle size range examined.

Also shown in Figure 4.8 are two other curves which show the effect of changing the values of the diffusivity (blue) and the chemical rate constant (grey). In each case the best-fit value was increased by 50 percent. Changing the diffusivity increased the calculated rate so that the predicted rate was always above the observed rate at times greater than zero. When the rate constant was increased, the initial rate was substantially overestimated, however, after about one day, the model fitted the experimental data well.

By using this method of estimating values of D_e and k, values were determined for each experiment for the range of particle sizes and temperatures examined. The results are summarised in Figures 4.9 and 4.10.

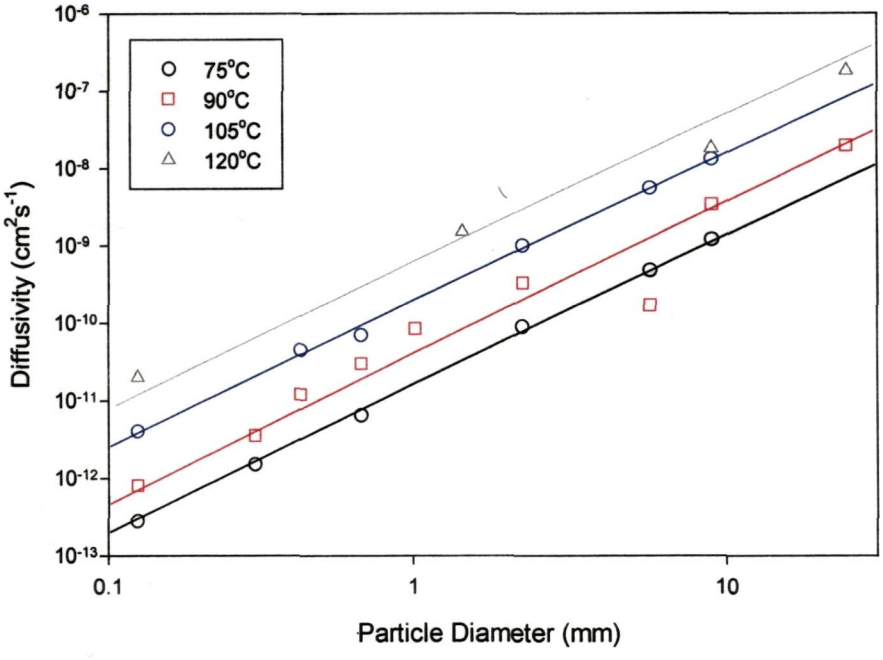

Figure 4.9. The dependence of the values estimated for the diffusivity, D_e, on particle size

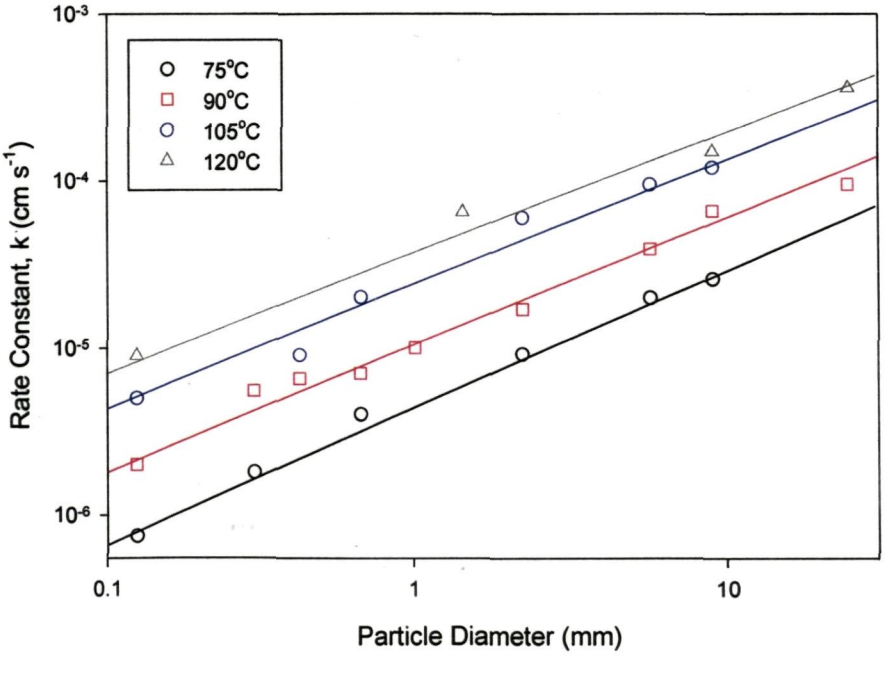

Figure 4.10. The dependence of the values estimated for the rate constant, k, on particle size

Both the diffusivity and the rate constant determined from the SCM increased with temperature. This is certainly expected behaviour in the case of the rate constant and plotting the logarithm of this value against $1/T$ for any particle diameter between about 0.125 and 9 mm yielded an average activation energy of about 60 kJ/mol. This value is slightly higher than but broadly consistent with the value of 45 kJ/mol determined by plotting the experimentally measured rates (see Effect of Temperature in Chapter 3).

Figure 4.9 shows that the diffusivity is also temperature dependent. Replotting these data as lnD_e against $1/T$ showed that the diffusivity also follows the Arrhenius relationship in the same way as the chemical rate constant.

Diffusion is generally less sensitive to temperature than the reaction rate (Levenspiel, 1993), but here, it appeared to be more affected than the rate constant. In this case the Arrhenius plot yielded an average activation energy of 90 kJ/mol for the diffusivity.

Figures 4.9 and 4.10 also show that the values of D_e and k required to fit the observed rate both increased with increasing particle size. Given that the chemical composition (see Chapter 3) and sample preparation of the coal used in these experiments were the same for the full particle range, it seems unlikely that the rate constant should change as a function of particle size. The apparent change in the rate constant with particle size is probably an artefact caused by the assumption that the reaction is confined to a narrow reaction front on a spherical surface. As was shown in Chapter 3, the actual reaction surface area is greatly underestimated if spherical geometry is assumed, which is the case with the shrinking core model. This means that the value used for k is not strictly the chemical rate constant but is in effect a curve-fitting parameter, although it would nevertheless be a function of the reaction rate.

To completely separate the rate constant from this parameter would require that the geometry of the reaction surface be more accurately known, which given the porous nature of coal would be difficult to achieve.

Increasing diffusivity with increasing particle size has been reported by Sevenster, 1959, and Wang *et al.*, 1999. Sevenster measured the diffusivity of oxygen in coal and found values within the range of about 4.5×10^{-14} to 1.1×10^{-11} $cm^2\ s^{-1}$. These values are within the range of the estimates made in the current study which were between approximately 10^{-13} and 10^{-7} $cm^2\ s^{-1}$. Sevenster did make the point, however, that the values determined were dependent upon the physical shape of the sample used to make the measurement. For large discs of material measured by Sevenster (effective diameter of 16 mm and 1 mm thick) much higher diffusivity was found compared to finely powdered coal. The difference was attributed to fine cracks present in the discs allowing gas to pass more easily through the coal. The implication of this finding is that larger particles, which are more likely to contain a system of microcracks, should show higher diffusivity. This is the trend observed in this study.

In a theoretical analysis of low temperature coal oxidation, Wang *et al.*, 1999 modelled the diffusivity in coal. Their work showed that, like Sevenster, the diffusivity increased with increasing particle size although the range of values reported were much higher than either Sevenster's or those found here. Their diffusivities were between about 10^{-8} and 10^{-6} $m^2\ s^{-1}$ (10^{-4} and 10^{-2} $cm^2\ s^{-1}$).

Despite the known shortcomings of assuming spherical geometry, the shrinking core model was nonetheless capable of providing excellent agreement with the observed rate data. This

suggests that the basis of the model, i.e. that the reaction proceeds by a combination of chemical and diffusion control at a contracting reaction front, may be reasonable. It may be, however, that the reaction front is contained within a diffuse zone rather than on a sharply defined front on the surface of the contracting spherical core. The values of k (and perhaps even D_e) determined for the Puxtrees coal fractions apparently include the effects of this "fuzziness".

Figures 4.9 and 4.10 show that $log(k)$ and $log(D_e)$ were both linear functions of the logarithm of particle diameter. Hence it should be possible to estimate the values of k and D_e for a particular particle size and, if the particle size distribution of the sample is known, estimate the rate for a full range sample. This was attempted for the full range samples measured at several temperatures. The particle size distribution of the full range samples measured at 22, 75, 90 and 105 °C were determined by sieve analysis and the results are shown in Table 4.1 below. The corresponding values of k and D_e for each fraction at 75, 90 and 105 °C were estimated from linear regression of the data shown in Figures 4.9 and 4.10. For the 22 °C sample, individual particle size fractions were not available so the values of k and D_e were estimated by assuming that:

- the linear particle size dependencies shown in Figures 4.9 and 4.10 were the same at 22 °C as they were at the higher temperatures and
- the effect of temperature could be estimated by applying the Arrhenius equation.

The rate for each particle size fraction shown in Table 4.1 was calculated using the SCM with the appropriate input parameters, then multiplied by the proportion of that size range in the sample. The calculated rates were then summed to give an overall curve for the complete sample.

Table 4.1. Particle size distribution of full-range samples

Mean Particle Diameter (mm)	*22 °C (%)*	*75 °C (%)*	*90 °C (%)*	*105 °C (%)*
28.45	21.6	0.0	12.5	7.7
22.25	26.1	5.0	20.4	32.7
17.55	10.7	6.7	18.6	3.6
14.6	7.9	7.4	17.2	13.9
11.6	7.0	17.9	12.6	11.7
9	4.0	18.0	6.0	10.0
7.35	4.8	12.0	3.6	4.5
5.725	2.3	9.6	2.4	2.7
3.775	5.9	10.8	1.5	3.7
2.25	3.0	5.0	1.5	2.5
1.44	2.0	2.0	0.9	1.4
1.105	1.1	1.4	0.8	1.1
0.675	1.5	1.8	1.0	1.6
0.4275	0.6	0.8	0.3	0.8
0.3025	0.6	0.6	0.3	0.7
0.125	0.9	1.0	0.5	1.1

The results of the model run for the 22 °C conditions are shown in Figure 4.11 along with the experimental data.

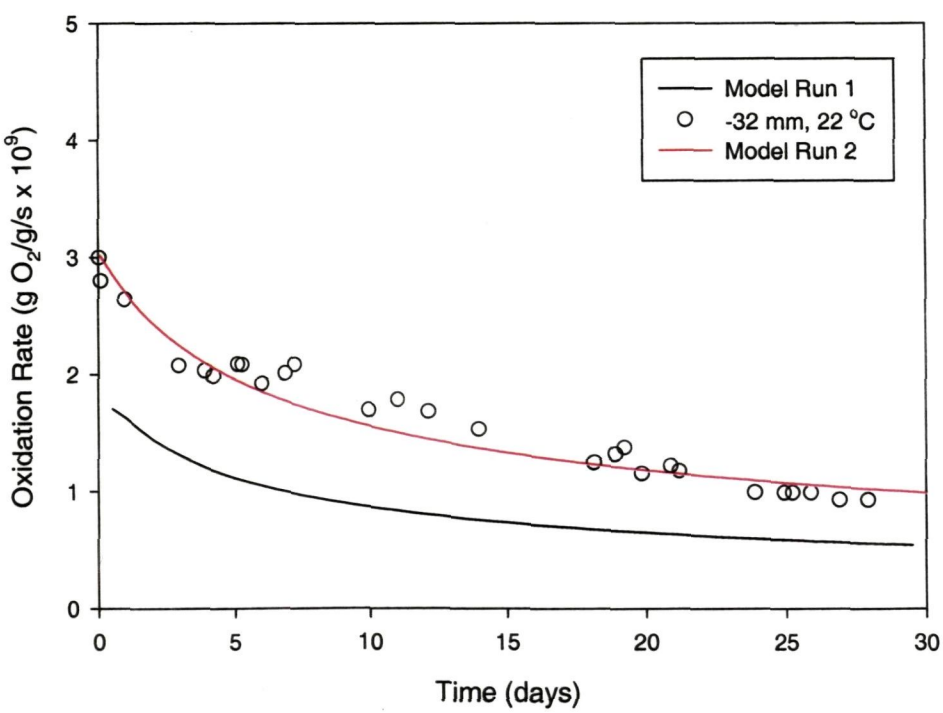

Figure 4.11. Comparison of measured rate data with rates calculated with the shrinking core model

Figure 4.11 shows the results of two modelling runs. The first (Run 1, shown as the black line) was performed using the method described above where the rates for individual size

fractions were summed to yield an overall rate. The rate curve obtained by this method underestimated the actual rate although the form of the curve was very similar to that of the measured data. It is likely that the difference between the observed and calculated rates is due to a compounding of errors associated with interpolation of the values of k and D_e. It is also possible that assuming the particle size dependence of k and D_e obeyed the same relationship as the higher temperatures may be invalid.

The second model run (Run 2, shown as the red line in Figure 4.11) was made by simply assuming a single mean particle diameter for the whole sample, i.e.16 mm. The values of k and D_e were selected by trial and error to obtain the best fit to the data and, as shown in Figure 4.11, the fit obtained was extremely good.

The results of the modelling for the other samples are shown in Figure 4.12.

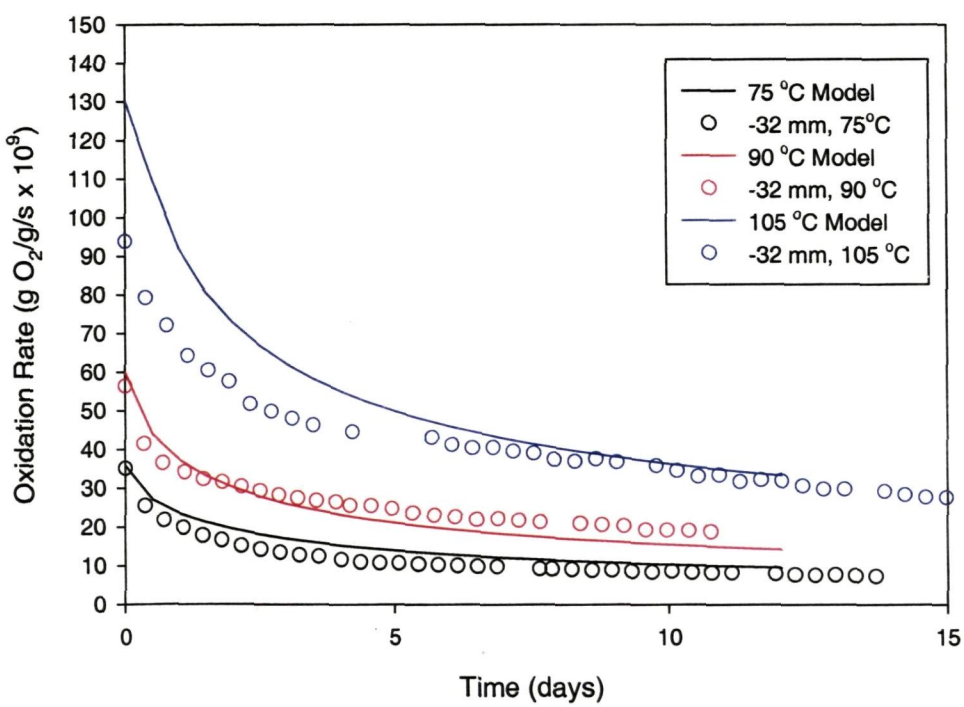

Figure 4.12. Comparison of measured data for 75, 90 and 105 °C with rates calculated with the shrinking core model

The fits obtained were generally better than for the 22 °C sample and particularly so for the 75 °C sample. The fit for the other two temperatures was reasonable although for the 105 °C sample, the rate was significantly overestimated at the start of the reaction. In these examples, the variation of k and D_e with particle diameter were measured and this is probably why the fit of the model is better than at 22 °C where these had to be estimated. However, like the 22 °C example shown in Figure 4.11, better fits were achieved for these runs if the a single mean particle diameter was assumed for the material then estimating k and D_e on this basis. Again, an almost perfect fit to the experimental results was obtained in each case.

The shrinking core model has been shown to be able to provide exceptionally good fit to the experimental data in almost all of the instances tried in this study. Although in the case of low temperature oxidation of coal its success seems to be at least partially due to empirical curve fitting, it does nevertheless have some theoretical basis. The main problem appears to be with the assumption that the reaction occurs on the surface of a sharply defined sphere where in reality, this is not the case.

A possible improvement to the shrinking core model when applied to coal was suggested by Carras (2001, personal communication). He proposed that each coal particle is itself made up of many, much smaller, spheres as shown in Figure 4.13. Such a structure would go some way to simulate the large-scale porosity of the coal.

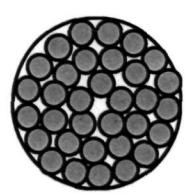

Figure 4.13. Structure of coal particles assumed in the modified shrinking core model

The small spheres are assumed to be shrinking cores as described above. The total rate for the individual coal particle is then given by the rate for a small sphere multiplied by the number of spheres in the particle. The number of spheres per particle is simply given by the volume of the particle divided by the volume of the sphere, which reduces to r_p^3 / r_s^3 where r_p is the radius of the particle and r_s is the radius of the small spheres.

In this model, oxygen can diffuse into the particle via the spaces between the smaller spheres. Oxygen will be consumed as it diffuses through the particle so that a concentration gradient will be established through the particle. This region corresponds to the diffuse oxidation layer discussed above. To model this layer would require a complex expression to calculate the oxygen concentration over the thickness of the layer, but in small diameter particles, where there is no particle size effect on the rate of oxidation, it can be assumed that the oxygen concentration is constant. In this situation, the concentration of oxygen seen by each small sphere will be C_{Og}. If the model is indeed a better approximation than the simple shrinking core, then the values needed for k and D_e should be constant, or nearly constant, over the entire particle size range.

To test this model the Visual Basic program used for the shrinking core model was modified slightly to calculate the number of spheres in each particle. The rates calculated were then compared to the experimental results as before.

It was necessary to estimate the radius of the small spheres representing grains within individual coal particles. A value of 0.001cm (10 μm) was selected after examination of several of the coal fractions by optical microscopy showed that although there was quite a range of grain sizes present, this value was within the appropriate order of magnitude.

As with the simple shrinking core model, when applied to individual particles, almost perfect fits to the data were obtained in each case. However, when model incorporating the small spheres was used, the rate constant and diffusivity values were much less affected by particle size. Figure 4.14 shows k and D_e as functions of particle size for 75 °C and 90 °C respectively.

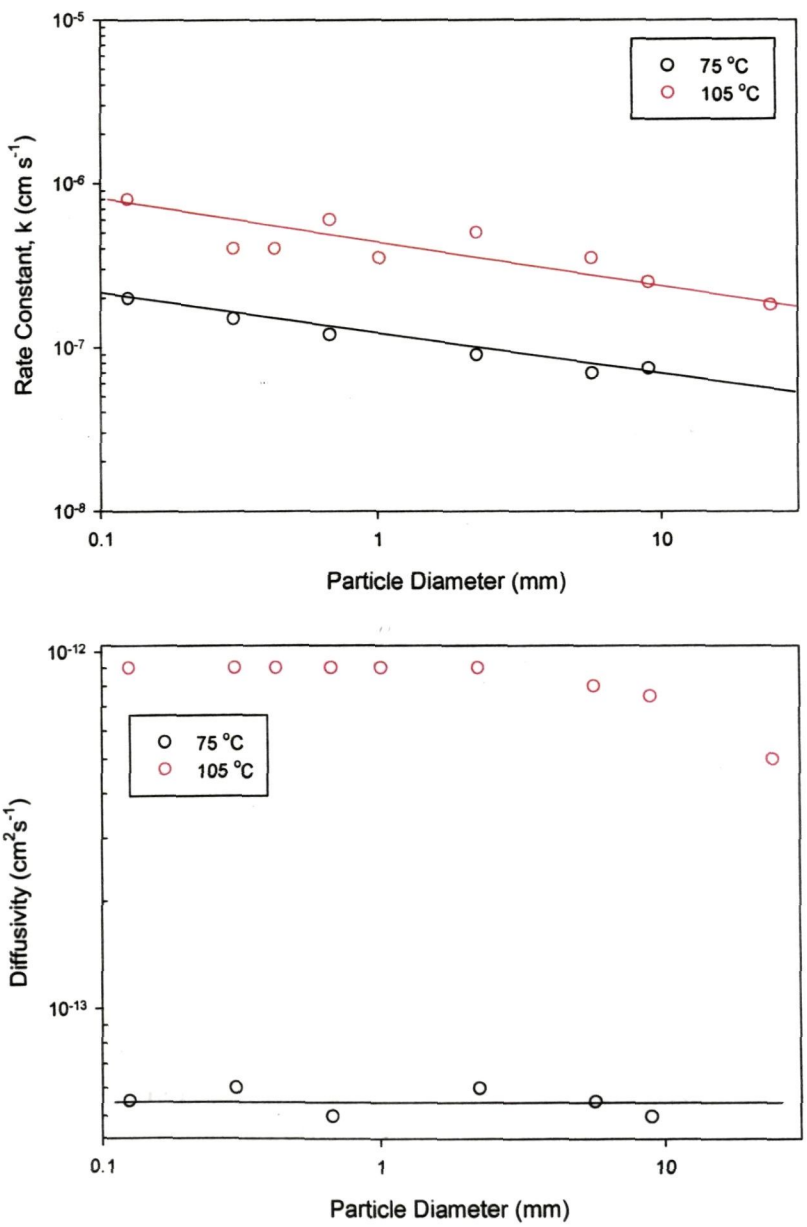

Figure 4.14. The dependence of the values estimated for the rate constant (a) and diffusivity (b) on particle size using the modified shrinking core model

The rate constant exhibited a decreasing trend with increasing particle size but the overall change over the particle size range was relatively small when compared to that observed when the original shrinking core model was applied. In that case k varied by a factor of more than 40 whereas here the change was about ten times less. The activation energy calculated from these rate constants (using the average value for k at each temperature) yielded a value of 45 kJ/mol that compared very well to the experimentally determined value of 45 kJ/mol.

In regimes where the measured rate showed no particle size dependence (i.e. at 75 °C or for particles less than about 1mm in diameter at higher temperatures), the value determined for the diffusivity was constant with particle size (Figure 4.14). However, under conditions where there was a rate dependence on particle size, the value of D_e began to decrease with increasing particle size. Under these conditions, the assumption that the oxygen concentration is constant throughout the particle is no longer valid.

In summary, the shrinking core model has been found to be able to fit experimentally measured oxidation rate data for Puxtrees coal over a wide range of temperatures and particle sizes. In its simplest form, where the oxidation reaction is considered to be confined to a spherical surface on each particle, the fit is due to some degree of adjusting the values of the rate constant and diffusion coefficient to compensate for the fact the reaction surface is really more complicated. The extension proposed by Carras appears to be a significant improvement since the values of the rate constant and diffusion coefficient do not need adjustment (to the same extent) to fit the data. This is not the whole answer, however, since in its present form it cannot adequately model regions where there is a pronounced particle size effect on the oxidation rate. This is probably due to the

assumption used that the oxygen concentration with in the particle is constant. Development of expressions to properly describe the true oxygen profile may overcome this limitation and improve this model even further.

4.3 The Pore Tree Model

As noted in the previous section dealing with the shrinking core model, it is apparent that the porous nature of coal needs to be considered when developing a model to describe the oxidation kinetics of coal. Porous models have, in fact, been developed in the past and have been applied to gasification kinetics (e.g. Bhatia and Perlmutter, 1980 and 1981). One such model, developed in the late 1970s (Simons and Finson, 1979; Simons, 1979), considers the pore structure within the coal or char particle to resemble a tree with the largest pores which reach the external surface of the particle being the tree trunks. Recently, Wang *et al.*, 1999, applied this pore-tree model to low temperature oxidation kinetics of coal and found that the particle size dependence predicted by the model agreed closely with data reported in the literature. Accordingly, it seemed logical to compare this model with the data set for the Puxtrees coal sample obtained in the current study.

4.3.1 Description of The Model

In the Simons model, oxidation is assumed to take place within pore structures that are open to the external surface of each particle (effective pores). Pores that do not open to the surface are considered to be blind and therefore do not participate in the oxidation process. The effective pores are assumed to have a tree-like structure with the largest diameter trunks reaching the surface of the particle while progressively smaller branches reach into the interior. For the purpose of the model it is further assumed that all of the tree structures are independent of each other.

On the surface of each particle are pore trunks ranging in radius from r_{min} to r_{max}.

The number of pores per unit of surface area was determined by Simons and Finson to be given by the function $g(r_p)$.

$$g(r_p) = \frac{(1-\phi)\theta}{2\beta\pi r_p^3} \tag{4.18}$$

where ϕ is the ratio of the volume blind pores to the total volume of the pore network, θ is the porosity of the coal and β is equal to $\ln(r_{min}/r_{max})$. Wang *et al.*, 1999, assigned a value of 12 to β in their modelling work. For a spherical particle, the total number of pores open to the surface is therefore equal to $4\pi a^2 g(r_p)$.

It has been shown (Simons and Finson, 1979; Wang *et al.*, 1999) that the maximum radius of the effective pores, r_{max}, is a function of the particle diameter, a, according to the expression:

$$r_{max} = \frac{2(1-\phi)^{1/3}\theta^{1/3}}{3K_0} a e^{-\gamma} \tag{4.19}$$

where K_0 and γ are constants. The constant K_0 is defined as the pore length to diameter ratio and γ is a coal specific parameter. Wang *et al.*, 1999, assigned values to these constants of 5 and 2.56 respectively.

Transport of oxygen through the pore structure can be either by molecular diffusion or Knudsen diffusion, depending on the pore radius. In larger diameter pores, molecular diffusion will be the dominant process. If the pores were straight cylinders parallel to the flow of gas, the oxygen flux across a unit of cross sectional area of a particle would simply be the molecular diffusion coefficient for oxygen, D_{O2}, multiplied by the voidage or porosity, θ, of the particle. However, the pores are much more likely to follow an irregular path which means that the oxygen molecules must travel further thereby reducing the flux. To account for this, a tortuosity factor, τ, is introduced (Satterfield, 1970) and the effective

diffusion coefficient (termed the continuum diffusion coefficient by Wang *et al.*), $D_{O2.eff}$, is given by:

$$D_{O2.eff} = \frac{D_{O2}\theta}{\tau} \tag{4.20}$$

Knudsen diffusion occurs in very fine capillaries where oxygen molecules collide with the walls of the pore more frequently than with other gas molecules. The high frequency of wall collisions has the effect of slowing the rate of diffusion. As the radius of the pore reduces, a point is reached where $D_{O2.eff}$ is equal to the Knudsen diffusion coefficient, $D_{O2.k}$.

The pore tree model considers that the overall oxidation rate can be limited by continuum diffusion (i.e. diffusion in larger pores), Knudsen diffusion or the rate of chemical reaction, with the controlling mechanism being determined by the pore size. Wang *et al.*, 1999, assigned pore size ranges to each of the three regimes:

- small pores with radii between r_{min} and r_1 in which the rate of oxidation is limited by the intrinsic rate of reaction,
- intermediate pores with radii between r_1 and r_2 where the rate is limited by Knudsen diffusion and
- large pores with radii between r_2 and r_{max} where the rate is limited by continuum diffusion.

Wang *et al.* showed that the rate of oxygen consumption under continuum diffusive control, $R_{CD}(r_p)$, Knudsen diffusive control, $R_{KD}(r_p)$, and chemical control, $R_{KL}(r_p)$, could be described by the following expressions:

$$R_{CD}(r_p) = \left(\frac{\rho_G D_{O2.eff} k}{2}\right)^{1/2} Y_{O2.s} 2\pi r_p^{3/2} \tag{4.21}$$

$$R_{KD}(r_p) = \left(\frac{\rho_G \theta \overline{V_{O2}} k}{3\tau}\right)^{1/2} Y_{O2.s} 2\pi r_p^2 \tag{4.22}$$

$$R_{KL}(r_p) = k\left(\frac{\theta}{\tau}\right)^{1/2} Y_{O2.s} s_p(r_p) \tag{4.23}$$

where $\overline{V_{O2}}$ is the mean thermal speed of oxygen molecules, $Y_{O2.s}$ is the mass concentration of oxygen at the particle's surface, k is the chemical rate constant and $s_p(r_p)$ is a function describing the surface area of the pore structure. To obtain the overall rate of oxygen consumption for a single coal particle, R_{O2}, Equations 4.21 to 4.23 are integrated for all pore radii within the ranges shown above and summed to yield:

$$\begin{aligned} R_{O2} = {} & k\left(\frac{\theta}{\tau}\right)^{1/2} Y_{O2.s} \frac{4\pi a^2 K_0 (1-\phi)^{2/3} \theta^{2/3}}{\beta r_{\min}} (r_1 - r_{\min}) \\ & + \left(\frac{\rho_G \theta \overline{V_{O2}} k}{3\tau}\right)^{1/2} Y_{O2.s} \frac{4\pi a^2 K_0 (1-\phi)\theta}{\beta} \ln\left(\frac{r_2}{r_1}\right) \\ & + \left(\frac{\rho_G D_{O2.eff} k}{2}\right)^{1/2} Y_{O2.s} \frac{8\pi a^2 K_0 (1-\phi)\theta}{\beta} \left(\frac{1}{r_2^{1/2}} - \frac{1}{r_{\max}^{1/2}}\right) \end{aligned} \tag{4.24}$$

The expression in Equation 4.24 provides the rate of oxygen consumption for an individual particle. To obtain the rate per unit mass, Equation 4.24 must be multiplied by the number of particles per unit mass, N, which is given by:

$$N = \left(\frac{3}{4\pi a^3 \rho_C}\right) \tag{4.25}$$

4.3.2 Results

Wang *et al.*, 1999, used their model to study effect of particle size on coal oxidation kinetics at 57 °C under various conditions of porosity and chemical reactivity. Their results showed that for large particles, the overall rate of oxidation was limited by continuum diffusion but as the particle size decreased, the controlling regime shifted to Knudsen

diffusion and then finally to chemical kinetics for very small particles. This is illustrated in Figure 4.15 which shows the fraction of the total rate contributed by each component as calculated by the model.

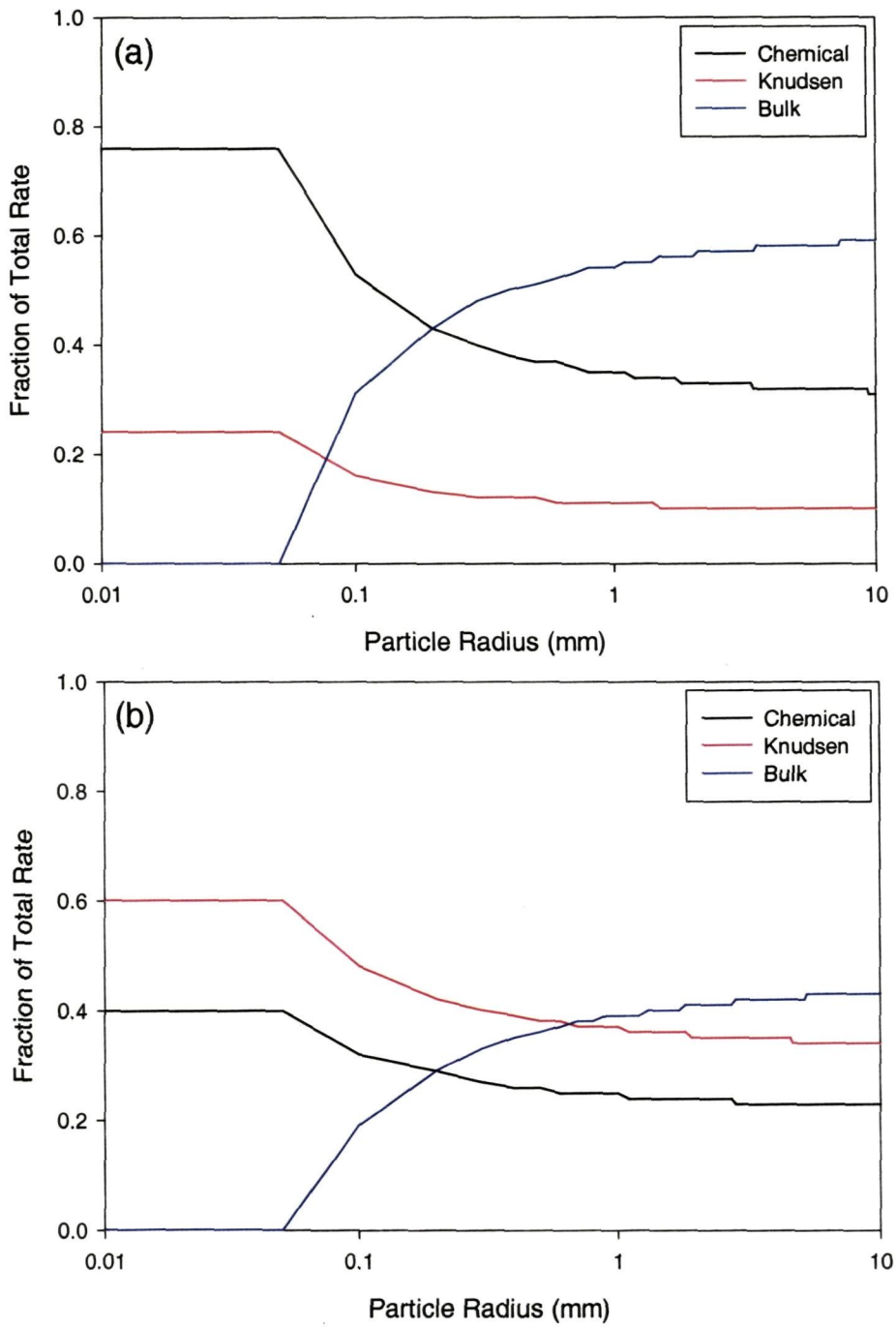

Figure 4.15. Fraction of total rate for chemical kinetics, Knudsen diffusion and bulk diffusion. (a) $k = 4 \times 10^{-7}$; (b) $k = 4 \times 10^{-6}$ cm s^{-1}

In Figure 4.15 (a), the rate constant, k, was set to 4.0 x 10^{-7} cm s^{-1} and under these conditions, the reaction was predicted to be under predominantly chemical control at particle radii less than about 0.07 mm. At larger particle sizes, the contribution to the overall rate from chemical kinetics begins to drop off with bulk diffusion becoming more significant.

In Figure 4.15 (b), the rate constant was set ten times higher than in the previous example to simulate a more reactive coal. In this case the model suggests that, for small particles, the overall rate limiting process has shifted from chemical control to Knudsen diffusion. As the particle size increases the rate controlling process tends towards bulk diffusion. These results agree with the experimental observations made here and elsewhere.

It is apparent from the description of the pore tree model that it is reliant upon a large number of input parameters and this can present a problem when attempting to compare the pore tree model with experimental data. Some of these parameters, such as the porosity, can be measured directly for particular coal samples. Others like the bulk diffusion coefficient for oxygen, D_{O2}, can be found in the literature but the majority cannot be measured easily or are empirical constants specific to each sample. As a result, fitting the model to data relies on adjusting the values used for each parameter until a best fit is obtained. This approach may be satisfactory when the model output is compared to experimental results, which effectively validates the model, however, if the model is to be used to predict rates in the absence of such data the level of confidence in the predictions is greatly reduced. This is particularly so given that the model is quite sensitive to a number of the parameters, especially k, r_{min}, γ and ϕ.

Notwithstanding the above, an attempt was made to compare the model with the measured rates for Puxtrees coal. In the modelling performed here, the parameters that could be measured with any degree of certainty were fixed, i.e. their values were not adjusted to improve the fit. Two input values that could be estimated were the chemical rate constant, k, and the porosity of the sample, θ.

The rate constant for the coal was estimated from $R_O = kC^n$ (Equation 3.1). As noted in Chapter 3, the rate at $t = 0$ must be chemically limited, so the initial value of R_O was used to determine the chemical rate constant for the reaction. The rate constant at 105 °C was found to be 1.01 x 10^{-6} cm s^{-1}.

The porosity of the sample was estimated from the mercury porosimetry results. These results showed decreasing porosity with increasing particle diameter, however, the model does not accommodate this trend so an average value of 0.05 mL/g was assumed. This equates to a value for θ of 0.065.

As noted above, the diffusion coefficient of oxygen, D_{O2}, is well known while the mass fraction of oxygen at the surface of a coal particle, $Y_{O2.s}$, is accurately known since it is the concentration of oxygen in air. The value of D_{O2} is temperature dependent but can be corrected by application of the following expression (Bird *et al.*, 1960):

$$D_{T2} = D_{T1}\left(T_2/T_1\right)^{1.823} \qquad (4.26)$$

where D_{T1} and D_{T2} are the diffusion coefficients at temperatures T_1 and T_2 respectively.

Table 4.2 shows the parameters used to achieve the best fit to the measured oxidation rates for Puxtrees coal at 105 °C.

Table 4.2. Input parameters used for pore tree model

Parameter	*Value Used*	*Comments*
k	1.01×10^{-6}	Estimated from results at 105 °C
θ	0.065	Measured directly from porosimetry
ϕ	0.95	From Wang *et al.*, not measured
τ	6	From Wang *et al.*, not measured
r_{min}	5×10^{-10} m	Arbitrarily set – value used by Wang *et al.*
β	12	Empirical constant used by Wang *et al.*
γ	2.56	Empirical constant used by Wang *et al.*
ρ_c	1300 kgm^{-3}	Measured directly by He pycnometry
D_{O2}	2.5×10^{-5} m^2s^{-1}	From CRC Handbook of Chemistry and Physics – corrected to 105 °C
$Y_{O2,s}$	0.235	21 % O_2 v/v in air equivalent to 23.5 % w/w

The results of the modelling run are shown in Figure 4.16 along with the measured rates for the Puxtrees coal at 105 °C and a Welsh coal (also at 105 °C) determined by Carpenter and Sergeant, 1966. Both the Puxtrees and Welsh coals exhibited decreasing oxidation rate with increasing particle size for large particles but the rate became independent of particle size at smaller radii.

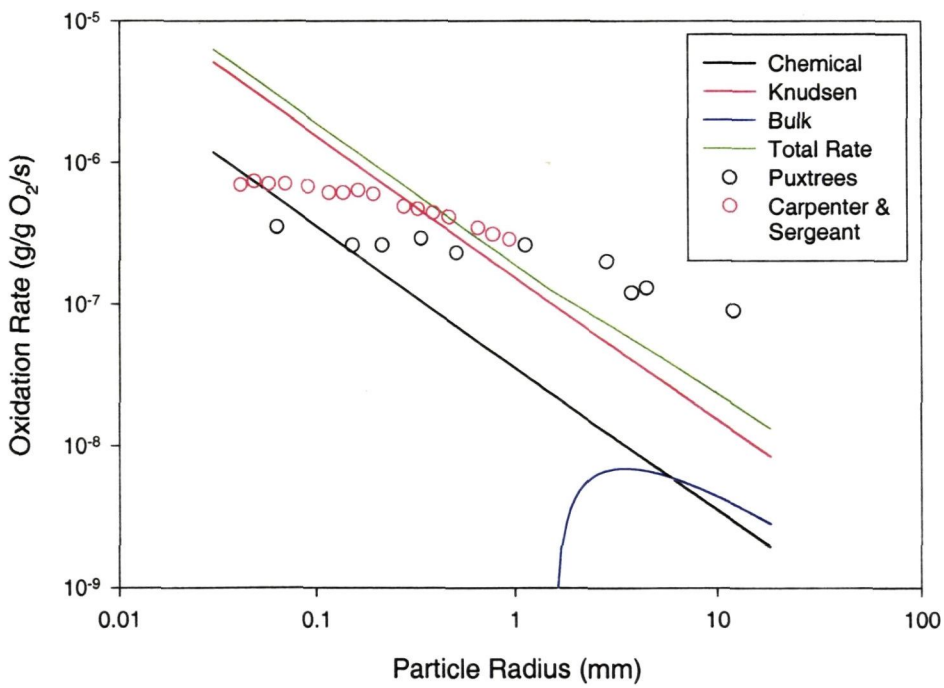

Figure 4.16. Oxidation rates predicted by the pore tree model for the chemical kinetics, Knudsen diffusion, bulk diffusion and overall rate using the parameters listed in Table 4.2. The data for Puxtrees coal were measured at t = 0 days at 105 °C.

The three components of the model, namely chemical kinetics, Knudsen diffusion and bulk diffusion are plotted separately together with the overall rate, which is the sum of these components. In the cases for chemical kinetics and Knudsen diffusion, the model has predicted that these components increase with decreasing particle radius over the entire particle range. The slope of each line in Figure 4.16 is –1 i.e. the rate is proportional to *1/a*. Examination of Equation 4.24 shows that for a given set of conditions, both the chemical and Knudsen components are functions of the square of the particle radius. When the rate per particle is multiplied by the number of particles per kilogram, which is a function of a^{-3}, we find that the rate becomes a function of *1/a*. Since all of the parameters in the chemical and Knudsen terms are constants under a given set of conditions they can be lumped together as a single constant. This works out to be the same form as the expression used by Akgün and Arisoy, 1994, (Equation 3.1) where an exponent of –1 suggests a reaction confined to the external surface of the particle.

The bulk diffusion component is also a function of a^2 but the rate curve in Figure 4.16 is very different from the others. In this case the rate is dependent upon r_{max} which is itself a function of a (Equation 4.24). The bulk diffusion curve shows an increase in rate with decreasing particle size but it reaches a maximum value then rapidly drops away. In fact, the values predicted for bulk diffusion were negative for small radius particles, which obviously, does not make physical sense.

The reason that negative values were generated by the model is that below a certain particle radius, the value calculated for r_{max} becomes less than r_2, hence the last term in Equation 4.24 must be negative. The physical significance of this is that the pores within particles smaller than this particular size are too small for bulk diffusion to occur so the oxidation rate must be controlled either by Knudsen diffusion of chemical kinetics.

Accordingly, a value of zero was ascribed to the bulk diffusion component when negative numbers were obtained.

The form of the overall rate curve (green line in Figure 4.16) is affected by the shape of the bulk diffusion component, but in general, the oxidation rate is predicted to increase with decreasing particle radius over the entire size range modelled. It is apparent from Figure 4.16 that the predicted rate provided by the model does not fit either the Puxtrees or Welsh coals. The particle size effect is also considerably over-estimated by the model. For example, the model predicted a rate of about 4.8 x 10^{-8} g O_2/g/s for a particle of 9 mm diameter while for a 0.12 mm particle, the rate was two orders of magnitude higher at 3.0 x 10^{-6} g O_2/g/s. For the Puxtrees coal, the increase in rate over this particle size range at 105 °C was much less: 1.3 x 10^{-7} g O_2/g/s at 9 mm to 3.5 x 10^{-7} g O_2/g/s at 0.12 mm. Adjusting the values of the non-fixed parameters did not significantly improve the fit.

The pore tree model was developed to describe the particle size effects on the rate of oxidation, but in its present form, does not include the time dependent nature of low temperature coal oxidation. Thus, even if it fitted the experimental data, it could at best only be applied to oxidation regimes that were under approximate steady state conditions. This may be the case after long periods of exposure to oxygen when the rate curve has levelled off but in the early stages of oxidation, where the rate of change is high, the model would not reliably predict the true oxidation rate.

4.4 References

Aharoni, C. and Ungarish, M., *J. Chem. Soc. Faraday Trans I.* 1976, **72**, 400-408.

Akgün, F. and Arisoy, A., *Combustion and Flame* 1994, **99**, 137-146.

Allardice, D. J., *Carbon* 1966, **4**, 255-262.

Bernaudat, L. MSc thesis Ecole des Mines d'Alès, 1999

Bird, R. B., Stewart, W. E. and Lightfoot, E. N. in Transport Phenomena 1960, J. Wiley and Sons, pp 507

Bhatia, S. K. and Perlmutter, D. D., *AIChE Journal*, 1980, **26**, 379-385

Bhatia, S. K. and Perlmutter, D. D., *AIChE Journal*, 1981, **27**, 247-254

Carras, J. N. and Young, B. C., *Prog. Energy Combust. Sci.* 1994, **20**, 1-15.

Denbigh, K. G. and Turner, J. C. R. in Chemical Reactor Theory 1971, Cambridge University Press, Cambridge, pp149.

Elovich, S. Yu. and Zhabrova, G. M. *Zh. Fiz. Khim.* 1939, **13**, 1761.

Handbook of Chemistry and Physics, Weast, R. C., ed 1970, 50th edition, CRC Rubber Company, Cleveland.

Harris, J. A. and Evans, D. G., *Fuel* 1975, **54**, 276-278.

Kaji, R., Hishinmura, Y. and Nakamura, Y., *Fuel* 1987, **66**, 154-157.

Khan, M. R., Everitt, C. E. and Lui, A. P., *Combustion and Flame* 1990, **80**, 83-93.

Levenspiel, O., in The Chemical Reactor Omnibook 1993, OSU Book Stores Inc, Corvallis, Oregon. pp 51-1.

Levenspiel, O., in Chemical Reaction Engineering, 3rd Ed. 1999, John Wiley and Sons, New York. pp 570.

Nordon, P., Young, B. C. and Bainbridge, N. W., *Fuel* 1979, **58**, 443

Pánek, P. and Taraba, B. Coal and its interaction with oxygen. Ostravské Univerzity Monograph 92, 1996

Roginsky, S. and Zeldovich, Ya. *Acta Physicochim.* 1934, **1**, 554-559

Sevenster, P. G., *Fuel* 1959, **38**, 403-418

Simons, G. A. and Finson, M. L., *Combust. Sci. Tech.* 1979, **19**, 217-225

Simons, G. A., *Combust. Sci. Tech.* 1979, **19**, 227-235

Smith, J. M., in Chemical Engineering Kinetics, 2nd Ed. 1970, McGraw-Hill, New York pp 576

Taylor, H. A. and Thon, N. J., *J. Am. Chem. Soc.* 1952, **74**, 4169-4173

Teng, H. and Hsieh, C-T., *Ind. Eng. Chem. Res.* 1999, **38**, 292-297

Wang, H., Dlugogorski, B. Z. and Kennedy, E. M., *Fuel* 1999, **78**, 1073-1081